

**The case for a directional dark matter detector and the status of  
current experimental efforts**

S. AHLEN,<sup>1</sup> N. AFSHORDI,<sup>22,30</sup> J. B. R. BATTAT,<sup>14</sup> J. BILLARD,<sup>11</sup> N. BOZORGNIA,<sup>3</sup>  
S. BURGOS,<sup>20</sup> T. CALDWELL,<sup>14, 21</sup> J. M. CARMONA,<sup>12</sup> S. CEBRIAN,<sup>12</sup> P. COLAS,<sup>4</sup>  
T. DAFNI,<sup>12</sup> E. DAW,<sup>25</sup> D. DUJMIC,<sup>14</sup> A. DUSHKIN,<sup>2</sup> W. FEDUS,<sup>14</sup> E. FERRER,<sup>4</sup>  
D. FINKBEINER,<sup>6</sup> P. H. FISHER,<sup>14</sup> J. FORBES,<sup>20</sup> T. FUSAYASU,<sup>15</sup> J. GALAN,<sup>12</sup>  
T. GAMBLE,<sup>25</sup> C. GHAG,<sup>5</sup> I. GIOMATARIS,<sup>4</sup> M. GOLD,<sup>17</sup> H. GOMEZ,<sup>12</sup> M. E. GOMEZ,<sup>7</sup>  
P. GONDOLO,<sup>28</sup> A. GREEN,<sup>19</sup> C. GRIGNON,<sup>11</sup> O. GUILLAUDIN,<sup>11</sup> C. HAGEMANN,<sup>17</sup>  
K. HATTORI,<sup>10</sup> S. HENDERSON,<sup>14</sup> N. HIGASHI,<sup>10</sup> C. IDA,<sup>10</sup> F. J. IGUAZ,<sup>12</sup> A. INGLIS,<sup>1</sup>  
I. G. IRASTORZA,<sup>12</sup> S. IWAKI,<sup>10</sup> A. KABOTH,<sup>14</sup> S. KABUKI,<sup>10</sup> J. KADYK,<sup>13</sup>  
N. KALLIVAYALIL,<sup>14</sup> H. KUBO,<sup>10</sup> S. KUROSAWA,<sup>10</sup> V. A. KUDRYAVTSEV,<sup>25</sup> T. LAMY,<sup>11</sup>  
R. LANZA,<sup>14</sup> T. B. LAWSON,<sup>25</sup> A. LEE,<sup>14</sup> E. R. LEE,<sup>17</sup> T. LIN,<sup>6</sup> D. LOOMBA,<sup>17</sup>  
J. LOPEZ,<sup>14</sup> G. LUZON,<sup>12</sup> T. MANOBU,<sup>9</sup> J. MARTOFF,<sup>26</sup> F. MAYET,<sup>11</sup> B. McCLUSKEY,<sup>25</sup>  
E. MILLER,<sup>17</sup> K. MIUCHI,<sup>10</sup> J. MONROE,<sup>14</sup> B. MORGAN,<sup>29</sup> D. MUNA,<sup>19</sup>  
A. St. J. MURPHY,<sup>5</sup> T. NAKA,<sup>16</sup> K. NAKAMURA,<sup>10</sup> M. NAKAMURA,<sup>16</sup> T. NAKANO,<sup>16</sup>  
G. G. NICKLIN,<sup>25</sup> H. NISHIMURA,<sup>10</sup> K. NIWA,<sup>16</sup> S. M. PALING,<sup>25</sup> J. PARKER,<sup>10</sup>  
A. PETKOV,<sup>20</sup> M. PIPE,<sup>25</sup> K. PUSHKIN,<sup>20</sup> M. ROBINSON,<sup>25</sup> A. RODRIGUEZ,<sup>12</sup>  
J. RODRIGUEZ-QUINTERO,<sup>7</sup> T. SAHIN,<sup>14</sup> R. SANDERSON,<sup>14</sup> N. SANGHI,<sup>17</sup>  
D. SANTOS,<sup>11</sup> O. SATO,<sup>16</sup> T. SAWANO,<sup>10</sup> G. SCIOCCA,<sup>14</sup> H. SEKIYA,<sup>27</sup> T. R. SLATYER,<sup>6</sup>  
D. P. SNOWDEN-IFFT,<sup>20</sup> N. J. C. SPOONER,<sup>25</sup> A. SUGIYAMA,<sup>23</sup> A. TAKADA,<sup>24</sup>  
M. TAKAHASHI,<sup>10</sup> A. TAKEDA,<sup>27</sup> T. TANIMORI,<sup>10</sup> K. TANIUE,<sup>10</sup> A. TOMAS,<sup>12</sup>  
H. TOMITA,<sup>1</sup> K. TSUCHIYA,<sup>10</sup> J. TURK,<sup>17</sup> E. TZIAFERI,<sup>25</sup> K. UENO,<sup>10</sup> S. VAHSEN,<sup>13</sup>  
R. VANDERSPEK,<sup>14</sup> J. A. VERGADOS,<sup>8</sup> J. A. VILLAR,<sup>12</sup> H. WELLENSTEIN,<sup>2</sup> I. WOLFE,<sup>14</sup>  
R. K. YAMAMOTO,<sup>14</sup> and H. YEGORYAN<sup>14</sup>

<sup>1</sup>*Boston University, Boston, MA 02215, USA*

<sup>2</sup>*Brandeis University, Waltham, MA 02453, USA*

<sup>3</sup>*University of California Los Angeles, Los Angeles, CA 90095, USA*

<sup>4</sup>*CEA Saclay, Cédex, France*

<sup>5</sup>*University of Edinburgh, Edinburgh, EH9 3JZ, UK*

<sup>6</sup>*Harvard University, Cambridge, MA, 02140, USA*

<sup>7</sup>*Universidad de Huelva, Campus El Carmen, 21071 Huelva, Spain*

<sup>8</sup>*University of Ioannina, Ioannina, Gr 451 10, Greece*

<sup>9</sup>*Institute of Particle and Nuclear Studies, KEK, Tsukuba, Japan*

<sup>10</sup>*Kyoto University Kitashirakawa-oiwakecho, Sakyo-ku, Kyoto, 606-8502, Japan*

<sup>11</sup>*Laboratoire de Physique Subatomique et de Cosmologie, Université Joseph Fourier Grenoble 1,  
CNRS/IN2P3, Institut National Polytechnique de Grenoble, 53, rue de Martyrs, 38026  
Grenoble, France*

<sup>12</sup>*Laboratorio de Física Nuclear y Astroparticulas, Universidad de Zaragoza, 50009 Zaragoza,  
Spain, and Laboratorio Subterráneo de Canfranc, Huesca, Spain*

<sup>13</sup>*Lawrence Berkeley National Laboratory, Berkeley, CA 94720, USA*

<sup>14</sup>*Massachusetts Institute of Technology, Cambridge, MA 02139, USA*

<sup>15</sup>*Nagasaki Institute of Applied Science, Nagasaki, Japan*

<sup>16</sup>*Fundamental Particle Physics Laboratory, Nagoya University, Japan*

<sup>17</sup>*University of New Mexico, Albuquerque, NM, 87131, USA*

<sup>19</sup>*New York University, New York, NY 10003, USA*

<sup>19</sup>*University of Nottingham, University Park, Nottingham, NG7 2RD, UK*

<sup>20</sup>Occidental College, Los Angeles, CA 90041, USA

<sup>21</sup>University of Pennsylvania, Philadelphia, PA 19104, USA

<sup>22</sup>Perimeter Institute for Theoretical Physics, Waterloo, ON N2L 2Y5, Canada

<sup>23</sup>Saga University, Saga, Japan

<sup>24</sup>Scientific Balloon Laboratory, ISAS, JAXA, Yoshinodai 3-1-1, Sagamihara, Kanagawa,  
229-8510, Japan

<sup>25</sup>University of Sheffield, Sheffield S3 7RH, UK

<sup>26</sup>Temple University, Barton Hall, Philadelphia, PA 19122, USA

<sup>27</sup>Kamioka Observatory, ICRR, The University of Tokyo, Higashi-Mozumi, Kamioka cho, Hida  
506-1205 Japan

<sup>28</sup>University of Utah, Salt Lake City, UT 84112, USA

<sup>29</sup>University of Warwick, Coventry, CV4 7AL, UK

and

<sup>30</sup>University of Waterloo, Waterloo, Ontario, N2L 3G1 Canada

<sup>14</sup>jbattat@mit.edu

We present the case for a dark matter detector with directional sensitivity. This document was developed at the 2009 CYGNUS workshop on directional dark matter detection, and contains contributions from theorists and experimental groups in the field. We describe the need for a dark matter detector with directional sensitivity; each directional dark matter experiment presents their project's status; and we close with a feasibility study for scaling up to a one ton directional detector, which would cost around \$150M.

*Keywords:* Dark matter; directional detection

PACS numbers

## 1. Theoretical motivation

Diverse astrophysical observations demonstrate that the majority of the matter in the Universe is in the form of non-baryonic cold dark matter.<sup>1</sup> Understanding the nature of the dark matter is one of the major outstanding problems of both astrophysics and particle physics.

The Weakly Interacting Massive Particle (WIMP) is a generically good dark matter candidate. A stable, weakly-interacting particle that was in thermal equilibrium in the early Universe will have roughly the right present-day density to comprise the dark matter. Furthermore, well-motivated extensions of the standard model of particle physics provide us with concrete WIMP candidates.<sup>2</sup> Supersymmetric models, in which every standard model particle has a supersymmetric partner, are motivated by the gauge hierarchy problem, the unification of coupling constants, and string theory. In these models, there is usually a conserved quantum number, R-parity (required to avoid proton decay), which renders the lightest supersymmetric particle (LSP) stable. In many cases the LSP is the lightest neutralino (a mixture of the supersymmetric partners of the photon, the Z and the Higgs) which is a good WIMP candidate. There has also been heightened interest recently in Universal Extra Dimension models, where the Lightest Kaluza-Klein particle is a WIMP candidate. A successful direct detection campaign will not only confirm the existence of dark matter, but will also probe high energy particle physics.

WIMPs can be detected in three ways: at particle colliders,<sup>3</sup> indirectly (astrophysically),<sup>2</sup> or directly in the laboratory.<sup>4</sup> The production and detection of WIMP-like particles at the LHC would be extremely exciting. As well as demonstrating that such particles exist in nature, it would provide information about their properties (mass and interactions). It would not, however, demonstrate that these particles are the dark matter in the Universe. In particular it would not show that the particles produced are stable on cosmological timescales. Astrophysical, indirect detection experiments attempt to detect the products of WIMP annihilation, e.g. high-energy gamma-rays, anti-matter and neutrinos, within the Milky Way and beyond. The detailed signals depend on the dark matter distribution, on details of the annihilation process, and on the propagation of charged particles in the Milky Way's magnetic field. As demonstrated by recent studies of the PAMELA positron excess,<sup>5</sup> a WIMP signal will need to be distinguished from astrophysical backgrounds from, for instance, pulsars and supernova remnants. Furthermore, the measurements themselves are very challenging, and at present, several indirect detection experiments, including ATIC and FERMI,<sup>6,7</sup> are in conflict with each other. This work focuses on the third option: direct detection, more specifically, on dark matter detectors that have sensitivity to the direction of arrival of dark matter particles.

### 1.1. *Direct detection*

Direct detection experiments<sup>8</sup> aim to detect WIMPs via their elastic scattering off of target nuclei in the laboratory. Specifically, they look for the energy deposited in a detector by a nuclear recoil from individual scattering events. Since WIMPs have a very small cross section with matter, these events are rare and the energy of the nuclear recoils is relatively small,  $\sim 10 - 100$  keV. Nonetheless, current experiments have already achieved the sensitivity required to rule out regions of supersymmetric parameter space consistent with all other observational and experimental constraints.<sup>9,10</sup> Neutrons, for instance from cosmic-ray muons or local radioactivity, can also produce nuclear recoils, which, on an event-by-event basis, cannot be distinguished from WIMP-induced nuclear recoils. Direct detection experiments minimize neutron backgrounds by operating deep underground, by using radiopure components, and by shielding the detectors appropriately. An unambiguous detection of WIMPs requires a smoking gun signal to demonstrate that the observed recoils are indeed due to WIMPs rather than neutrons or other backgrounds.

There are three potential WIMP signals, namely the time, direction, and target nucleus dependence of the energy spectrum of the recoils. Due to the kinematics of elastic scattering, the shape of the energy spectrum depends on the mass of the target nuclei, and, for spin-independent interactions (where the WIMP interacts coherently with the nucleus), the normalisation of the spectrum is proportional to the square of the mass number. In principle, the consistency of energy spectra measured in two or more experiments with different target nuclei could demonstrate

4 *Battat et al.*

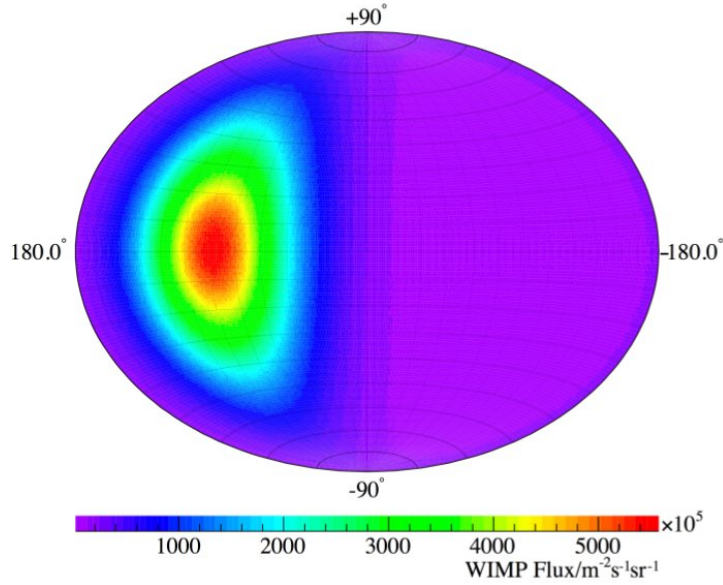


Fig. 1. Hammer-Aitoff projection of the WIMP flux in Galactic coordinates. A WIMP mass of 100 GeV has been assumed (from Ref. 12).

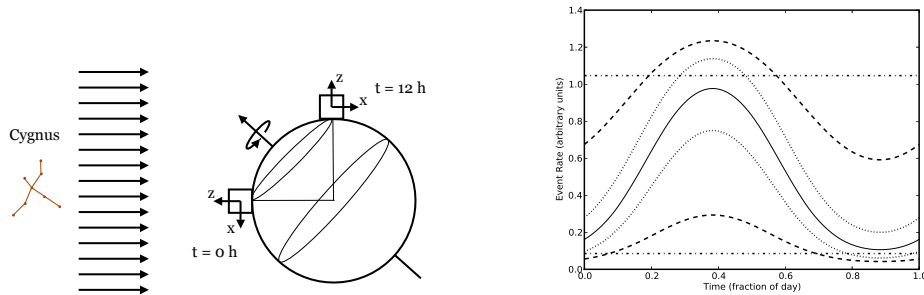


Fig. 2. (left) The daily rotation of the Earth introduces a modulation in recoil angle, as measured in the laboratory frame. (right) Magnitude of this daily modulation for seven lab-fixed directions, specified as angles with respect to the Earth’s equatorial plane. The solid line corresponds to zero degrees, and the dotted, dashed, and dash-dot lines correspond to  $\pm 18^\circ$ ,  $\pm 54^\circ$  and  $\pm 90^\circ$ , with negative angles falling above the zero degree line and positive angles below. The  $\pm 90^\circ$  directions are co-aligned with the Earth’s rotation axis and therefore exhibit no daily modulation. This calculation assumes a WIMP mass of 100 GeV and  $\text{CS}_2$  target gas. (from Ref. 13).

the WIMP origin of the dark matter interaction candidate events.<sup>11</sup> This is often referred to as the materials signal. In practice, this would require the detection of a large number of events with both targets (in order to measure the energy spectra), the operation of experiments in similar background environments, and accurate calculations of the nuclear form factors.

### 1.2. *Temporal modulation*

The Earth's yearly orbit about the Sun produces an annual modulation of the nuclear recoil energy spectrum.<sup>14,15</sup> The Earth's net speed with respect to the Galactic rest frame is largest in summer (when the Earth's orbital vector is aligned with the Sun's orbital vector). This boosts the WIMP speed distribution in the laboratory frame towards higher speeds and hence leads to a larger number of high energy recoils (and a deficit of low energy recoils). Because the Earth's orbital speed is small compared to the Sun's speed with respect to the Galactic rest frame, the amplitude of the annual modulation is small, of order a few percent. Therefore its detection requires the stable operation of a large detector mass over a long period of time. Furthermore, the details of the annual modulation signal, in particular its phase and amplitude, are somewhat dependent on the ultra-local (sub-milliparsec) WIMP velocity distribution. The DAMA/LIBRA collaboration has measured an annual modulation in their event rate.<sup>16</sup> Even with ample statistics and even though the modulation amplitude, frequency, and phase are consistent with the expectations of Galactic dark matter, the DAMA/LIBRA measurement has not been widely interpreted by the physics community as evidence for dark matter, in part because of the possibility that an annual modulation of background, rather than WIMP flux, could fake the signal. It is clear that the wide acceptance of a dark matter detection claim requires a less ambiguous signature.

### 1.3. *Direction modulation*

The Earth's motion with respect to the Galactic rest frame also produces a direction dependence in the recoil spectrum.<sup>17</sup> The peak WIMP flux comes from the direction of solar motion, which happens to point towards the constellation Cygnus (see e.g. Fig. 1). Assuming a smooth WIMP distribution, the recoil rate is then peaked in the opposite direction. In the laboratory frame, this direction varies over the course of the sidereal day due to the Earth's rotation (see Fig. 2), thereby providing a robust signature of the Galactic origin of a WIMP signal. As shown in Fig. 2, the number of recoils along a particular direction in the laboratory frame will change over the course of the day. The amplitude of this modulation depends on the relative orientation between the lab-fixed direction and the spin axis of the Earth, with no modulation along directions parallel to the Earth's spin axis. No known background can mimic this signal. The lab-frame recoil directions can be rotated into galactic coordinates to produce a 2D skymap of recoil directions. A directional detection experiment can then look for anisotropies in the galactic skymap of nuclear recoils.

The expected directional signal is far larger than the annual rate modulation. For a simplified, but representative WIMP halo model (the isothermal sphere), the event rate in the forward direction is roughly an order of magnitude larger than that in the backward direction. In this halo model, a detector capable of measuring the nuclear recoil momentum vector (the axis and direction of the recoil, also called the "head-tail" of the track) in 3-dimensions, with good angular resolution, could

distinguish a WIMP signal from isotropic background with only  $O(10)$  events.<sup>18,12</sup> Directional detection therefore provides the best opportunity to unambiguously demonstrate the Galactic origin of a nuclear recoil signal.

#### 1.4. *Non-spherical halo models*

Signal calculations for direct detection experiments (both directional and non-directional) are usually based on the isothermal sphere halo model, containing a smooth WIMP distribution with an isotropic Maxwellian speed distribution, truncated at the galactic escape velocity.<sup>11</sup> Plausible astrophysical and particle physics deviations from this baseline model can produce other interesting signals in directional experiments.

This standard halo model is unlikely to be a good approximation to the real Milky Way halo. The details of the directional signal depend on the ultra-local WIMP distribution which is not currently well-known. Numerical simulations have finite resolution and can only probe the dark matter distribution on kiloparsec scales. For reference, the Earth-Sun distance is  $5 \mu\text{pc}$ , and in one year, the Solar System moves approximately 0.2 milliparsec along its galactocentric orbit. It has been argued that on the sub-milliparsec scales probed by direct detection experiments, the dark matter distribution may not be completely smooth.<sup>19</sup> In the extreme case of a velocity distribution consisting of a small number of discrete peaks, the recoil spectrum would still be highly anisotropic, albeit not peaked in the direction opposite to Cygnus, and possibly time dependent on a 1–10 year timescale. It is, however, extremely unlikely that the WIMP induced recoil spectrum would be completely isotropic (this would require a dark matter halo with bulk co-rotation). The dependence of the directional recoil spectrum on the WIMP velocity distribution in fact provides an opportunity. With a larger sample of events, a directional detector would be able to do WIMP astronomy, reconstructing the ultra-local WIMP velocity distribution and hence shedding light on the dynamics of the Milky Way halo by finding streams clustered in momentum space. This would be highly complementary to the mapping of the full six-dimensional phase-space distribution, (positions and velocities), of the stellar component of the Milky Way by astronomical surveys (such as SDSS, and in the future, GAIA).

#### 1.5. *Inelastic scattering*

There has been interest recently in inelastic WIMP scattering (the iDM scenario). This happens if the WIMP effectively has a ground state and an excited state separated by  $\sim 100$  keV, which can be the case in models with a new dark sector force, composite dark matter or mirror dark matter.<sup>21</sup> This scenario is compatible with all current direct detection experiments, including DAMA. Inelastic scattering is qualitatively different from elastic scattering. The event rate at low energies is suppressed, due to the energy required to excite the higher energy state. Furthermore, the nuclear recoils are more correlated with the initial direction of the incident

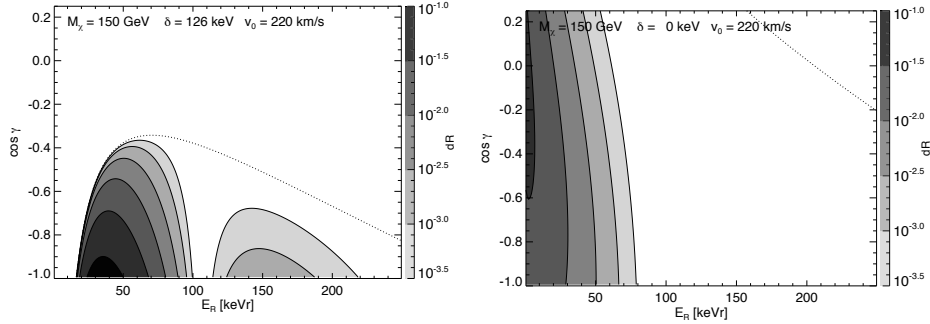


Fig. 3. Differential rates  $dR/(dE_R d\cos\gamma)$  for the benchmark models given in Ref. 20 with  $v_{esc} = 500$  km/s, for (a) inelastic and (b) elastic scattering. In each case, the differential rate is normalized so that the total rate is unity. Outside the region indicated by the dashed line, scattering events are kinematically forbidden. Note that inelastic scattering preserves directional information better than elastic scattering.

WIMP, thereby producing a stronger directional signal than in the case of elastic scattering (see Fig. 3 and Ref. 20). A directional experiment with a heavy target (required for sufficient kinetic energy in the center of momentum frame) could provide a crucial test of the iDM scenario even with a modest exposure ( $\sim 10^3$  kg-day).<sup>20</sup>

In summary, the direction dependence of the direct detection rate provides a powerful tool for distinguishing WIMP-induced nuclear recoils from background events, and can unambiguously demonstrate the Galactic origin of a dark matter signal. A detector capable of measuring the nuclear recoil vectors in 3-dimensions could detect the directional signal with only of order 10 events. With a large exposure it would be possible to do “WIMP astronomy” and measure the ultra-local WIMP velocity distribution. Directional detection can also test the inelastic scattering scenario.

## 2. Status of experimental efforts

Directional dark matter experiments face several common challenges. Most importantly, the detector must accurately reconstruct low-energy (tens of keV) recoil tracks in its active volume. In diffuse gas detectors, these track lengths typically only extend a few millimeters, which necessitates a readout system with high spatial resolution. Of particular interest is the head-tail, or vector direction, of the recoil (see Section 1.3). By leveraging the non-uniform energy loss of recoiling nuclei as a function of recoil distance ( $dE/dx$ ) experiments can measure the head-tail of a recoil.

Several groups have well-established research programs devoted to directional dark matter detection. Various target materials and readout techniques have been employed and evaluated. Sections 3-7 present the current status of, and recent results from five directional dark matter detection experiments (DRIFT, DMTPC, NEWAGE, MIMAC and Nuclear Emulsions). For convenience, Table 1 summarizes

Table 1. Summary of existing directional dark matter detection experiments. TPC stands for Time Projection Chamber, NITPC stands for negative-ion TPC, and SI and SD refer to spin-independent and spin-dependent WIMP-nucleon interactions. The column labeled “head-tail” specifies whether the experiment has successfully demonstrated head-tail sensitivity. The last column lists the active volume for each experiment.

Collaboration	Technology	Target	Interactions	Head-tail	Readout	V (m <sup>3</sup> )
DRIFT	NITPC	CS <sub>2</sub> , CS <sub>2</sub> -CF <sub>4</sub>	SI/SD	yes	MWPC 2D + timing	1
DMTPC	TPC	CF <sub>4</sub>	SI/SD	yes	Optical (CCD) 2D	0.01
NEWAGE	TPC	CF <sub>4</sub>	SI/SD	no	μPIC 2D + timing	0.03
MIMAC	TPC	<sup>3</sup> He/CF <sub>4</sub>	SI/SD	yes	Micromegas 2D + timing	0.00013
Emulsions	emulsions	AgBr	SI/SD	no	Microscope 3D	N/A

these experiments. In addition, Sections 8 and 9 describe the status of R&D efforts on novel detector readout schemes: silicon pixel chips and micromegas.

Even as these experiments work toward developing ton-scale detectors with directional sensitivity, there is near-term science that can be achieved with more modest target masses. For example, an exposure of 0.1 kg-year with CF<sub>4</sub> gas (equivalent to three months of live time with a one cubic meter detector filled to 75 Torr) would improve current constraints on the spin-dependent cross section by a factor of  $\sim 50$  over current limits. In addition, in the iDM scenario (see Section 1.5), an exposure of  $\sim 3$  kg-yr with a heavy target (e.g. Xenon) and directionality could either rule out or support the DAMA/LIBRA signal under the inelastic dark matter scenario.

Finally, it has been shown<sup>22,23</sup> that WIMP spin-independent and spin-dependent cross sections with nucleons can be uncorrelated: meaning that a given supersymmetric dark matter candidate may have a relatively large spin-dependent nuclear cross section, but a very weak spin-independent cross section. Therefore even modest constraints on the spin-dependent cross section can rule out SUSY models that will remain out of reach of traditional dark matter direct detection experiments. Fig. 4 demonstrates this by showing the spin-dependent (left) and spin-independent (right) cross sections for a class of SUSY models. The curve on the left plot shows the hypothetical sensitivity of a directional experiment that uses <sup>3</sup>He as a target gas. The points above the curve could be ruled out by such an experiment. The spin-independent plot shows that models ruled out by the <sup>3</sup>He-based experiment have a broad range of spin-independent cross sections, extending below  $10^{-12}$  pb, well below the sensitivity of the next generation of traditional direct detection experiments. Although these plots are made for <sup>3</sup>He gas, similar results follow for other targets with high spin-dependent sensitivity (e.g. fluorine).

### 3. DRIFT – Scale-up tests with low background and head-tail discrimination

The Directional Recoil Information From Tracks (DRIFT) dark matter collaboration at Boulby has, since 2001, pioneered construction and operation underground of low background directional TPCs at the 1 m<sup>3</sup> scale with Multi-wire Proportional Counter (MWPC) readout using negative ion (NITPC) CS<sub>2</sub> gas to suppress dif-



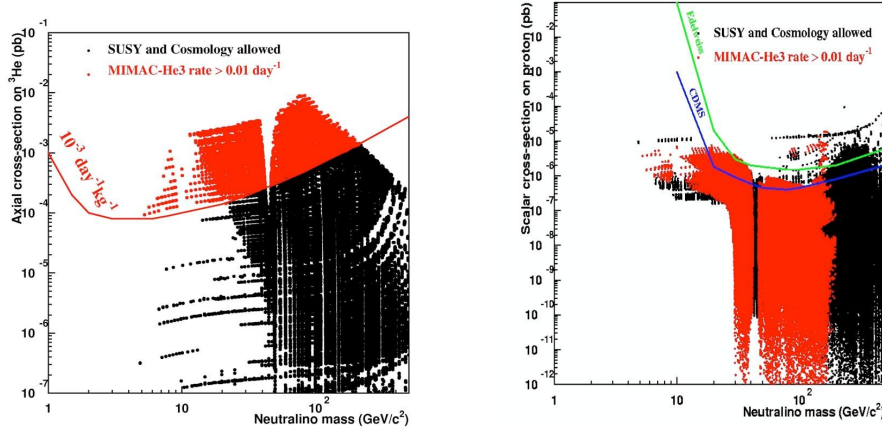


Fig. 4. SUSY non-minimal models, calculated with the DarkSusy code.<sup>24</sup> (left) Axial (spin-dependent) cross section on nucleon as a function of the neutralino mass. (right) Scalar (spin-independent) cross section of the same models. In red the models giving an axial cross section higher than a projected exclusion curve for an experiment with 10 kg of  $^3\text{He}$ . These models are compared with the exclusion plots of scalar experiments (not updated). There are models, in red on the right, which require a level of sensitivity that will be very difficult to achieve with scalar experiments.<sup>22,23</sup>

fusion without magnetic fields.<sup>25,26</sup> The NITPC concept, as demonstrated first in DRIFT I, allows larger drift distances ( $> 50$  cm) than is feasible with conventional gases like  $\text{CF}_4$ , thereby reducing the required readout area and hence cost.<sup>27,28</sup> Operation with  $1\text{ m}^2$  MWPC readout planes allows the study of realistic size detectors underground with near-conventional technology.

In DRIFT, the ionization generated from recoil events (mainly S recoils) goes to create tracks of  $\text{CS}_2$  negative ions. Under the influence of an applied electric field, the negative ions drift to one of the two back-to-back MWPC planes for readout. The MWPCs include two orthogonal layers (x and y) of 512 20 micron wires with 2 mm spacing. Wires are grouped to reduce the number of readout channels. Reconstruction is feasible in 3D using timing information for the z direction (perpendicular to the x-y plane of wires). Additional R&D is underway to allow absolute z positioning, though some z positioning is feasible already through pulse shape analysis. Calibration is undertaken typically every 6 hours using internal  $^{55}\text{Fe}$  sources (one for each MWPC) that are shielded by an automated shutter system when not in use.

The Boulby program, particularly with the second generation  $1\text{ m}^3$  scale DRIFT IIa-d experiments since 2006 (see Fig. 5 and Ref. 29), has recently made progress on the practical understanding of all background types for directional TPCs operated underground, on scale-up issues such as safety and backgrounds, and on directional sensitivity, for instance demonstrating for the first time sensitivity to recoil direction

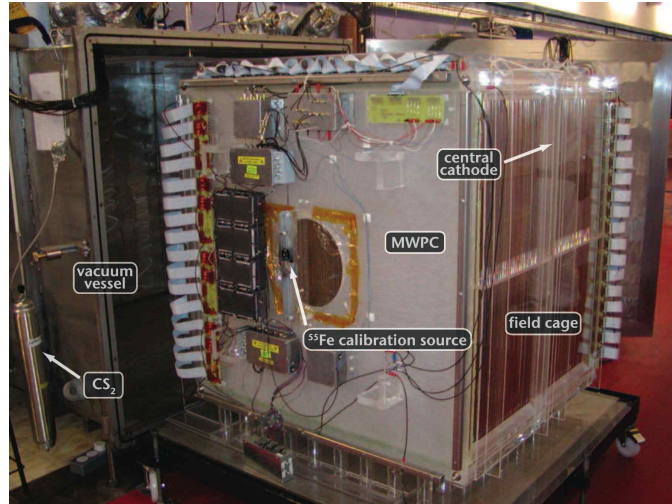


Fig. 5. DRIFT IIb detector at Boulby mine. Two back-to-back TPCs each with a 50 cm drift distance, share a common vertical central cathode. Readout is done with two 3-layer MWPCs with 2 mm wire spacing. Operation is with negative ion  $\text{CS}_2$  gas at 40 Torr (170 g target mass).<sup>29</sup>

sense (head-tail discrimination) at low energy (47 keV S recoil).<sup>30</sup>

DRIFT recognizes that micromegas/strip readout can offer improvements in resolution which could, for instance, allow for higher pressure operation.<sup>31</sup> Initial small-scale studies have already confirmed that micromegas technology can work with negative ion  $\text{CS}_2$  gas (see Fig. 6).<sup>32,33</sup> The parallel progress made by MI-MAC/CAST (Grenoble, Darmstadt) in developing larger area full x-y readout devices in the laboratory with  $\text{CF}_4$ , including the necessary advanced electronics, is therefore very well matched to the DRIFT activity, complementing the practical experience of using the  $\text{m}^3$ -scale low pressure TPCs of DRIFT underground, and offering a collaborative route to demonstrating feasibility of micromegas readout at this larger volume. It builds also on the long-standing Sheffield/Darmstadt collaboration to show that DRIFT could be used for axion detection (see Section 3.3).<sup>34</sup> Relevant advances from DRIFT are outlined in the following sections (DRIFT is a UK/US collaboration).

### 3.1. Background rejection and event fiducialisation

The strong gamma background rejection capability of the low-pressure TPC technology with  $\text{CS}_2$ , typically  $> 10^8$ , together with maintenance of recoil detection efficiency  $> 50\%$  (calibrated with neutron sources) has been demonstrated by DRIFT II.<sup>35,36</sup> More significant is the discovery, understanding and mitigation of specific radon related background events that are an issue for the scale-up of any dark matter directional TPC.<sup>37</sup> Called Radon Progeny Recoils (RPRs), the origin of this important background in TPCs has been identified by us as mainly  $^{210}\text{Po}$

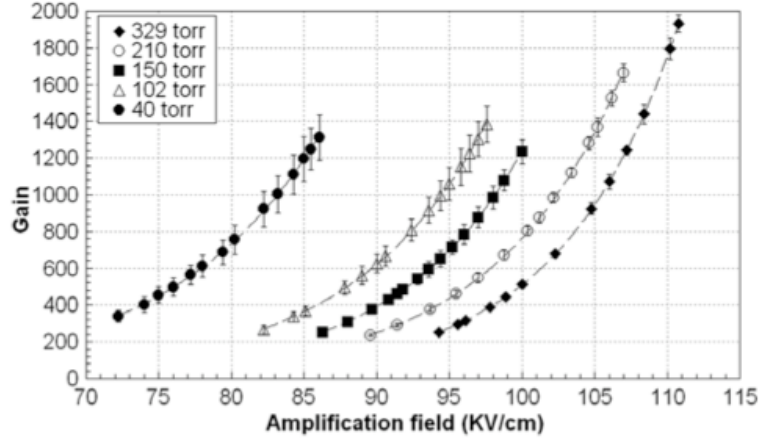


Fig. 6. Example gain curves for the operation of a 36 x 36 mm bulk micromegas device with negative ion  $\text{CS}_2$  gas. From Ref. 33.

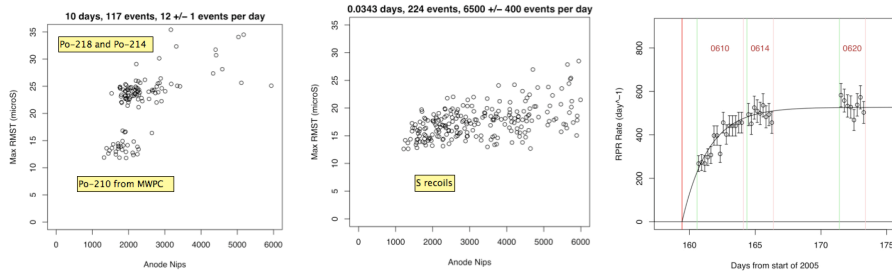


Fig. 7. (left) Identified RPR low background events in DRIFT IIb. (middle) Low energy ( $> 40$  keV) calibration sulphur recoils from a neutron exposure (gamma rejection is  $> 10^8$ ). (right) Rise in  $^{210}\text{Po}$  RPR events with time following new gas fill fitted to expectation of RPR hypothesis. From Ref. 39.

recoils from the central cathode (see Fig. 7). We have developed new radon reduction procedures via nitric acid cleaning,<sup>38</sup> new fiducialisation analysis software, and a material selection process using a radon emanation facility built for this purpose. Our latest analysis demonstrates that these techniques reduce the number of RPRs by a factor of 3000, yielding a background rate in DRIFT IIb of  $\sim 1$  event per week above threshold (40 keV recoil) for a target mass of 167 g  $\text{CS}_2$ . Further ideas for reducing the remaining RPRs to insignificant levels are being investigated by DRIFT. Elimination of RPRs would be a major breakthrough for directional technology towards zero background.

### 3.2. Directionality including recoil sense (head-tail)

3D track reconstruction of nuclear recoils, electrons and alphas has now been demonstrated in DRIFT II (see Fig. 8).<sup>37,40,41</sup> The latter has been shown also to provide a

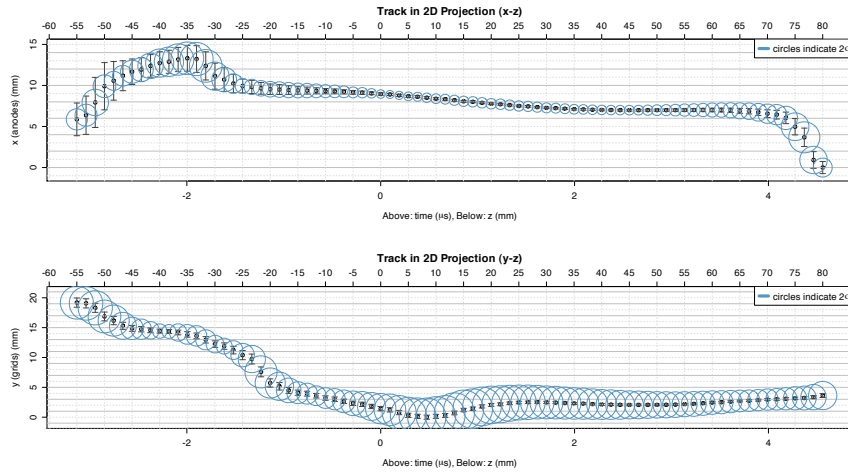
12 *Battat et al.*

Fig. 8. Example 3D reconstruction ( $x$ - $z$  and  $y$ - $z$  projections) of a  $\sim 100$  keV S recoil in DRIFT IIb (circle sizes indicate the amount of deposited charge).

powerful diagnostic for background identification via particle  $dE/dx$  and range. However, a simpler 2D analysis also provides directional sensitivity (see Fig. 9 left).<sup>37</sup> There is a strong dependence of the 3D directional resolution on the track orientation relative to the  $x$ ,  $y$ ,  $z$  planes, on the absolute position in  $z$ , and on the recoil energy. Results of a simulation to illustrate this are shown in Fig. 10. Here, shadings represent the probability that the reconstruction is accurate to within 30 degrees of the true recoil direction for events parallel to the  $x$ - $y$  plane.<sup>37</sup>

It has been a long-time goal of directional detectors to determine (both theoretically and experimentally) whether the absolute direction of low energy (10s of keV) recoils can be seen. This has the potential to improve directional sensitivity by a factor of 10, through better correlation with galactic motion.<sup>12</sup> DRIFT has recently succeeded in this, demonstrating for the first time at realistic recoil energies that a clear head-tail asymmetry is observable (see Fig. 9 right).<sup>30</sup> Our recent work with gas theorist Akira Hitachi now also provides a rigorous theoretical basis for this, in agreement with measurements.<sup>42</sup>

### 3.3. Low threshold operation (3 keV) and particle identification including axions

The potential advantages in WIMP detection of achieving a low (sub-10 keV) recoil and electron energy threshold in a low pressure TPC have been recognized.<sup>27,29,28,43</sup> However, simulation work through the Sheffield/Darmstadt collaboration has also established the potential in this situation for axion detection, specifically KK axions (see Fig. 11).<sup>44,34</sup> More recently, we have shown experimentally that recoil thresholds  $< 3$  keV (without directional information) are indeed feasible in the  $1 \text{ m}^3$

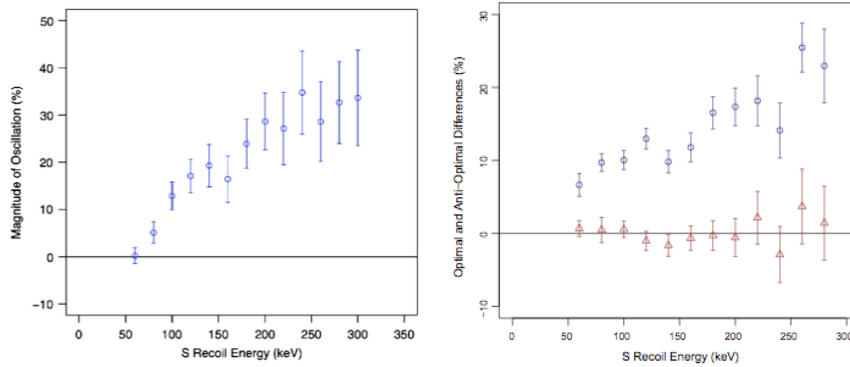


Fig. 9. Low energy (down to 40 keV S recoil) directional signals from DRIFT IIb: (left) ratio of  $\Delta z$  to  $\Delta x$  ranges vs energy and (right) head-tail asymmetry measured by the proportion of observed in first and second half of recoil tracks projected in the  $z$  direction. From Ref. 37.

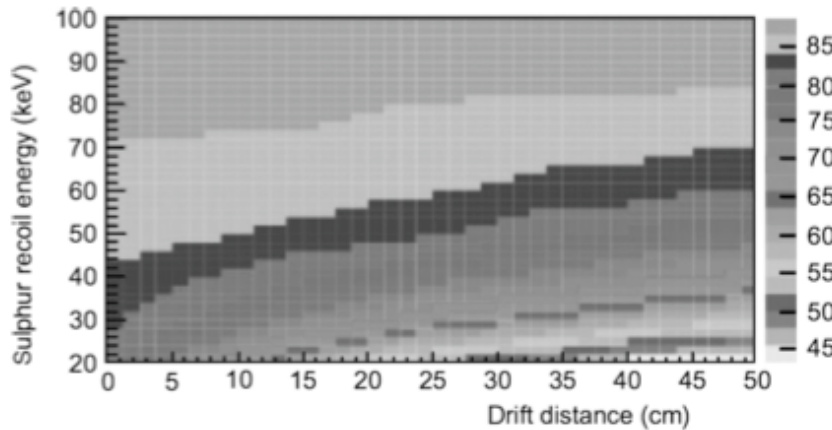


Fig. 10. Simulated angular reconstruction accuracy for DRIFT-II. Shading denotes the probability that the recoil direction is reconstructed within 30 degrees of the known initial direction.

DRIFT volume, even with the current commercial electronics.<sup>45</sup> Fig. 11 shows a sample  $^{55}\text{Fe}$  spectrum (6 keV photopeak) taken from a full-volume exposure to the 1 m<sup>3</sup> DRIFT IIb CS<sub>2</sub> detector at Boulby. Data filtering algorithms were applied here, however new low-noise electronics developed at Sheffield should eliminate the need for this, opening prospects for S recoil trigger thresholds of 2–4 keV (lower than achieved by the ionisation/phonon bolometric dark matter experiments).<sup>45</sup> The current results (see Fig. 11) after pulse filtering indicate sensitivity to electrons at 1.2 keV and hence S recoils at 3.5 keV, the former with a resolution of 17.5% at the 5.9 keV peak.

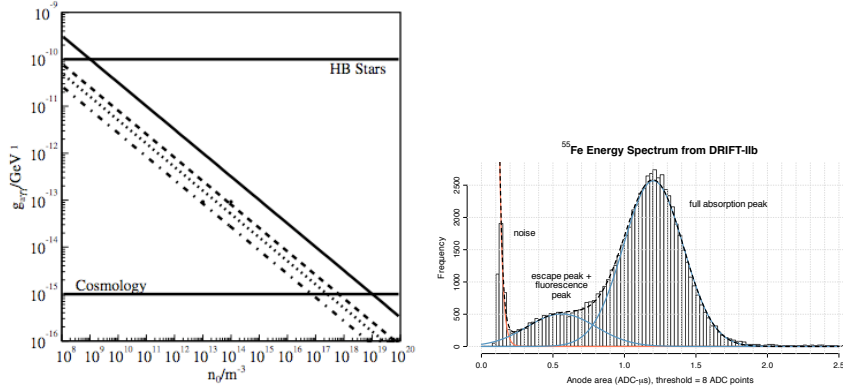
14 *Battat et al.*

Fig. 11. (Left) predicted sensitivity of 1 m<sup>3</sup> CS<sub>2</sub> TPC at 0.2 bar to KK axions based on tracking of low energy electrons (see Ref. 8) and (right) measured energy threshold in DRIFT IIb using <sup>55</sup>Fe. From Ref. 45.

### 3.4. Alternative target nuclei and spin-dependent sensitivity

It has long been postulated that CS<sub>2</sub> can be used as a “carrier” for other gases such that alternative target nuclei can be used while maintaining the low diffusion advantages of the negative ion drift CS<sub>2</sub>.<sup>46</sup> Our studies with low pressure CS<sub>2</sub> mixtures in small chambers have now shown excellent gain and stability behavior with various gases including CF<sub>4</sub> and He (see Fig. 12).<sup>31,47</sup> This opens a clear avenue for operation with F and <sup>3</sup>He targets for spin-dependent sensitivity incorporating the reduced diffusion offered by the CS<sub>2</sub>. In pure CS<sub>2</sub>, the diffusion constant is reduced to thermal levels.<sup>26</sup> Recent measurements of  $W$ , the average energy required to generate an electron-ion pair, and mobility with CS<sub>2</sub>-CF<sub>4</sub> mixtures demonstrate operation in negative ion mode with CF<sub>4</sub> and suggest near thermal diffusion, though more measurement are needed to confirm this.<sup>47</sup> Based on these results, and those above, we show in Fig. 12 predicted limits for spin-dependent interactions for a 1 m<sup>3</sup> CS<sub>2</sub>-CF<sub>4</sub> mixture.

### 3.5. Towards scale-up with low background

The DRIFT detectors at Boulby have also demonstrated that safe operation with long term stability (operation for many months with minimal gain shifts, trip-outs or alarms) is feasible at the m<sup>3</sup> scale underground. This is an essential step towards scale-up designs. However, of critical importance now is a deeper understanding of backgrounds relevant to large volume, more sensitive directional TPCs, particularly of muon, muon-induced neutron and detector neutron backgrounds, for instance to determine the need for an external bulk neutron veto. Significant preliminary work has been covered by our simulation activity (with GEANT4 and FLUKA) on muon-induced neutrons<sup>48,49,50</sup> backed by dedicated measurements at Boulby to understand the muon flux at low and high energy,<sup>51,52</sup> and the relevant fast neutron

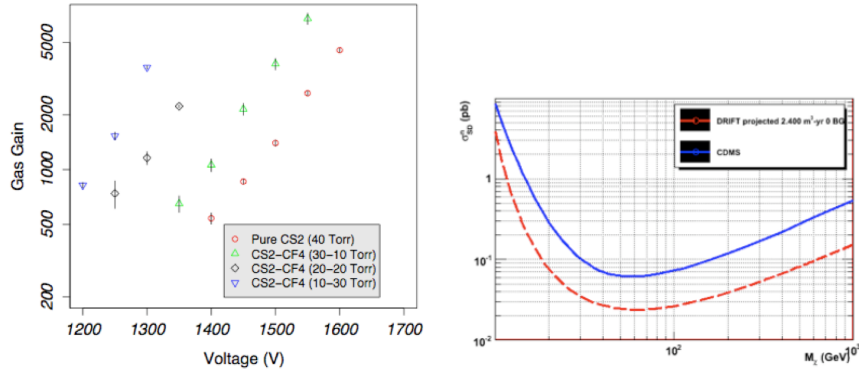


Fig. 12. (left) Gain curves measured for various  $\text{CS}_2\text{-CF}_4$  mixtures confirming operation in a small chamber; (right) predicted spin-dependent WIMP-neutron sensitivity with a 10 day exposure of  $1 \text{ m}^3$  with a 50%-50% mix of  $\text{CS}_2$  and  $\text{CF}_4$ . The projected 90% CL limits assume zero background and 100% efficiency.

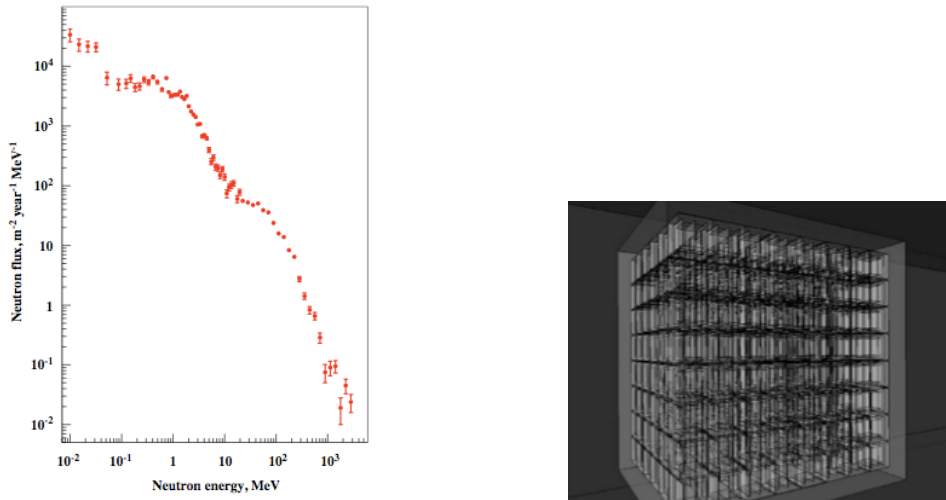


Fig. 13. (left) Simulated energy spectrum of muon-induced neutrons entering a (right) model multi-module low pressure TPC (vessel/gas boundary). From Ref. 36.

flux.<sup>53</sup> Fig. 13 shows example simulation flux predictions for a multi-module scaled-up TPC array.<sup>36</sup>

#### 4. The Dark Matter Time Projection Chamber (DMTPC) collaboration

The Dark Matter Time Projection Chamber (DMTPC) collaboration has developed and operated a 10-liter gas-based directional dark matter detector. The current instrument consists of a dual TPC, filled with  $\text{CF}_4$  gas at  $\sim 75$  Torr. Proportional

scintillation from the avalanches is read out with two CCD cameras. The charge on the TPC anode is also measured. With this instrument, DMTPC has demonstrated head-tail sensitivity for neutron-induced recoils above 100 keV, and an angular resolution for track reconstruction of  $15^\circ$  at 100 keV. An 18-liter detector is currently under construction and will be run underground at the Waste Isolation Pilot Plant (WIPP) at a depth of 1600 meters water equivalent.

#### 4.1. *Detector description and performance*

The 10-liter DMTPC detector is shown in Fig. 14. The dual-TPC is housed inside a stainless steel vacuum vessel. The drift region is defined by a woven mesh cathode, typically at a potential of -5 kV, separated from a wire mesh (28  $\mu\text{m}$  wire, 256  $\mu\text{m}$  pitch) ground grid 20 cm away. The vertical drift field is kept uniform to within 1% by stainless steel field-shaping rings spaced 1 cm apart. An amplification region is formed between the ground grid and a copper-clad G10 anode plane (at 720 V) which are separated from each other by 500  $\mu\text{m}$  using resistive spacers (currently fishing line). A charge amplifier connected to the anode measures the ionization generated by a particle moving through the detector. A CCD camera images the proportional scintillation light generated in the amplification region. The CCD camera and readout electronics are located outside of the vacuum vessel. The mesh-based amplification region allows for two-dimensional images of charged particle tracks.

With a  $\text{CF}_4$  pressure of 75 Torr, gas gains of approximately  $10^5$  are routinely achieved with minimal sparking (see Fig. 15). The energy resolution of the charge readout is 10% at 5.9 keV (measured with an  $^{55}\text{Fe}$  source), and is 15% at 50 keV for the CCD readout (measured with an alpha source, see Fig. 15). Since the stopping  $dE/dx$  in the detector is much smaller for electrons than for nuclear recoils, the surface brightness of an electron track is dimmer, and electron tracks are easily distinguished from nuclear recoils. This is shown in Fig. 16. The gamma rejection of our detector was measured to be  $> 10^6$  using an 8  $\mu\text{Ci}$   $^{137}\text{Cs}$  source.<sup>54</sup>

#### 4.2. *$\text{CF}_4$ gas properties*

$\text{CF}_4$  has many advantages as a target gas for a dark matter search in a gaseous TPC. First, it has good sensitivity to spin-dependent interactions because of its unpaired proton. In addition, it is a good counting gas, allowing gas gains in excess of  $10^5$ . The scintillation spectrum of  $\text{CF}_4$  has significant emission in a broad ( $\sim 100$  nm wide) peak centered at 625 nm.<sup>56</sup> This spectrum is well-matched to the peak quantum efficiency of CCDs. In addition, the measured transverse diffusion of electrons in  $\text{CF}_4$  is less than 1 mm for a 20 cm drift length at  $E/N = 12 \times 10^{-17}$  V  $\text{cm}^2$  (e.g. 300 V/cm at 75 Torr in the detector). Also, there is negligible electron attachment over a 20 cm drift.<sup>55</sup>



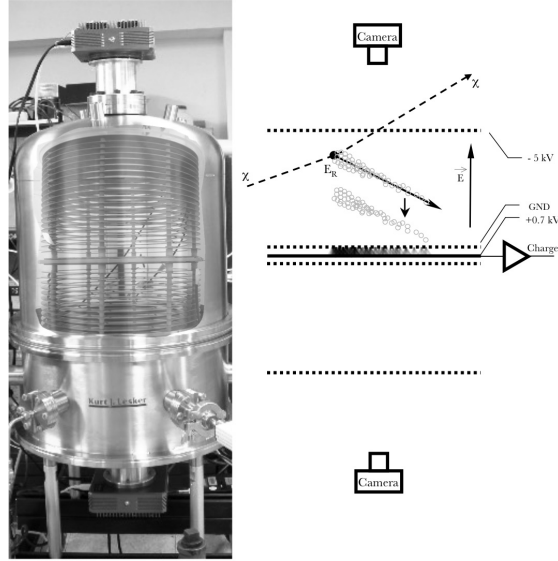


Fig. 14. (left) Photograph of the 10-liter DMTPC detector with an image of the dual TPC overlaid to provide an artificial glimpse inside the vacuum vessel. The CCD cameras (top and bottom) each image an amplification region. The stack of stainless steel field shaping rings condition the drift fields. (right) A schematic representation of a WIMP-nucleus elastic scattering event in the detector.

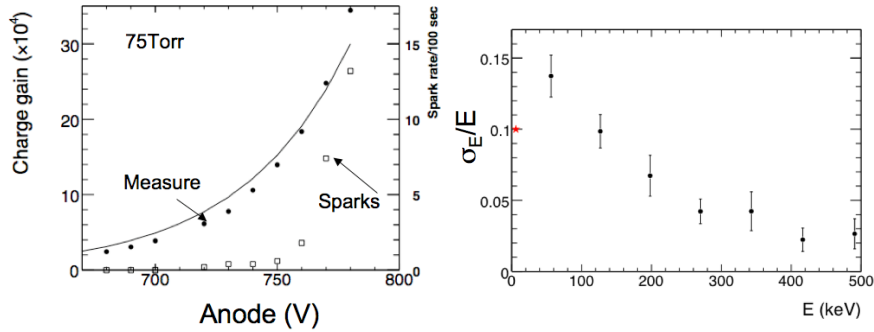


Fig. 15. (left) Gas gain and spark rate as a function of anode voltage for a mesh-based TPC filled with 75 Torr of  $CF_4$ . The gas gain is measured from the charge collected from an  $^{55}Fe$  source. (right) The energy resolution of the charge readout at 5.9 keV (star) and the CCD readout (circles) for energies above 50 keV. Fig. from Ref. 55.

### 4.3. Head-tail measurements

As described in Ref. 57, the DMTPC collaboration has demonstrated the ability to measure the head-tail effect (the vector direction of a recoil) on an event-by-event basis for energies down to 100 keV. In that work, a  $^{252}Cf$  neutron source irradiated a mesh-based detector filled with  $CF_4$  at 75 Torr. The CCD camera acquired 6,000

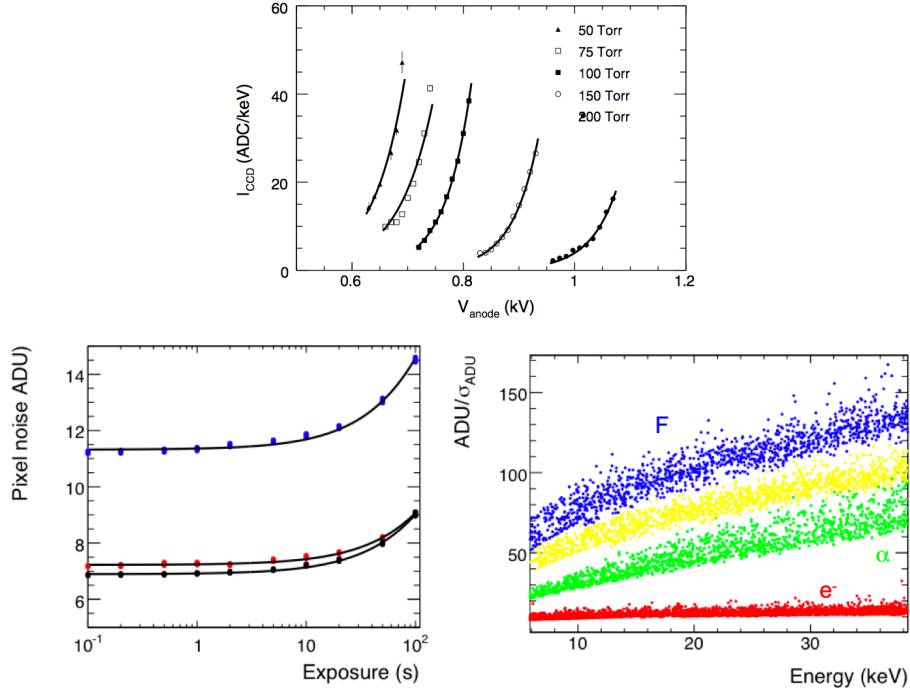


Fig. 16. (top) System gain for the TPC with CCD readout in units of ADU per keV as a function of amplification region voltage for  $\text{CF}_4$  at various pressures. (bottom left) CCD noise as a function of exposure time, obtained with the shutter closed. The three curves correspond to different CCD cameras with different gain settings (photoelectrons per ADU). In all cases, the CCD read noise (zero exposure) is approximately 12 electrons (rms). For exposure times less than  $\sim 10$  seconds, the CCD dark noise is negligible. (bottom right) Monte Carlo predictions for the signal-to-noise ratio in a charged particle track. Electrons, with smaller stopping, travel long distances and generate lower surface brightness tracks compared with nuclear recoils which lose their full energy over a shorter distance.

one-second-exposure images, and 19 of these images contained a candidate nuclear recoil. Two examples of these neutron-induced nuclear recoils are shown in Fig. 17. In these images, the nuclear recoil axis and direction (head-tail) is clearly visible for each event.

Fig. 18 shows the measured and predicted range vs. energy for these events. The recoil direction can be measured from the light profile along the recoil track. For the candidate nuclear recoils, a dimensionless skewness parameter  $S = \mu_3/\mu_2^{3/2}$  is constructed, where  $\mu_2$  and  $\mu_3$  are the second and third moments of the light distribution. In our data set, kinematics constrain all nuclei to be forward scattered and therefore have negative skewness. Fig. 18 shows that the skewness can be correctly reconstructed down to 100 keV.

For a set of nuclear recoils, the true forward-backward asymmetry is  $A = (F - B)/(F + B)$ , where  $F$  and  $B$  are the number of forward and backward recoils,

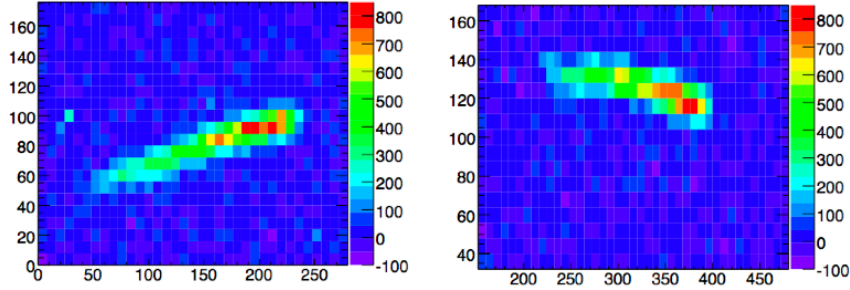


Fig. 17. Sample neutron-induced nuclear recoil candidates. The neutrons were incident from the right. The head-tail is evident from the light distribution along the track. In these images, 100 pixels corresponds to 6 mm. Figures taken from Ref. 58.

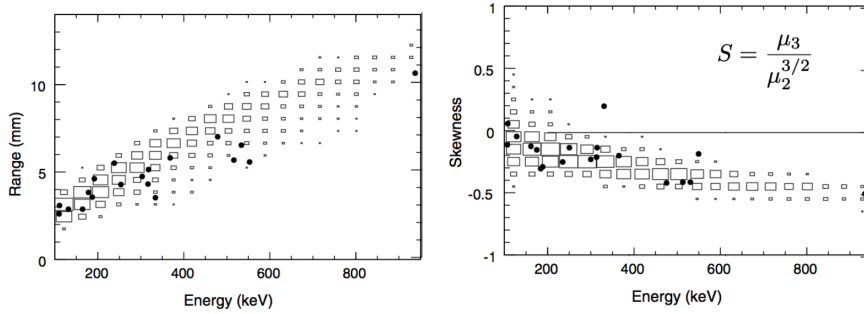


Fig. 18. (left) The observed (points) and predicted (box-histogram) range-energy relationship for candidate nuclear recoils induced by  $^{252}\text{Cf}$  neutrons in the detector; (right) the skewness parameter, a measure of the head-tail effect, for the candidate recoils. A negative skewness parameter indicates that the head-tail was correctly reconstructed. Figures taken from Ref. 58.

respectively. The measurement error on  $A$  scales like  $\sigma_A \sim 1/\sqrt{N Q_{HT}}$ , where  $N$  is the total number of measured recoils.  $Q_{HT}$  is a head-tail reconstruction quality factor:

$$Q_{HT}(E_R) \equiv \epsilon(E_R) \left( \frac{N_{good} - N_{wrong}}{N_{good} + N_{wrong}} \right)^2 \quad (1)$$

where  $E_R$  is the recoil energy,  $\epsilon$  is the (recoil energy dependent) head-tail reconstruction efficiency, and  $N_{good}$  and  $N_{wrong}$  are the number of events with head-tail correctly and incorrectly reconstructed. Monte Carlo studies show that  $Q_{HT}$  exceeds 50% above 140 keV (see Fig. 19). The nuclear recoil direction can be reconstructed with an angular resolution of  $15^\circ$  at 100 keV (see Fig. 19).

#### 4.4. From surface run to underground

The 10-liter detector was operated for two long runs in a basement lab at MIT for durations of six and three weeks. To ensure gas purity during the long runs,

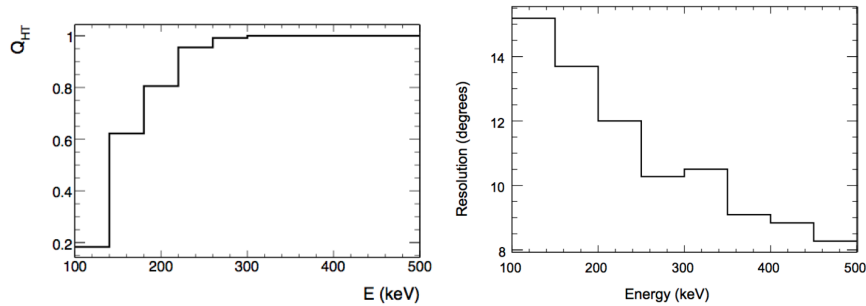
20 *Battat et al.*

Fig. 19. (left) The head-tail quality factor  $Q_{HT}$ , as computed from Monte Carlo studies. (right) The angular resolution for track reconstruction as a function of energy, also from Monte Carlo. Figures taken from Ref. 58.

the vessel was evacuated and then re-filled with 75 Torr of  $\text{CF}_4$  each day. Over a 24 hour period, the system gain was stable to 1%. An analysis of the data from these runs to study the backgrounds in the detector will be the subject of an upcoming publication.

The DMTPC collaboration is currently constructing a second detector, similar in target mass to the existing detector, to deploy underground to the Waste Isolation Pilot Plant (WIPP) in New Mexico, USA. At WIPP (1.6 km.w.e. depth), less than one neutron-induced event per year is expected in the detector. In addition, because the new detector will be constructed from highly radiopure materials in a low-radon environment, we expect a significant reduction of alpha backgrounds.

#### 4.5. DMTPC future goals

In addition to the preparation for WIPP, DMTPC is working on several aspects of detector R&D. A program is underway to achieve full volume fiducialization by measuring the z-coordinate of an interaction in the TPC. This can be achieved through the detection of primary scintillation light or from an analysis of the charge pulse profile on the cathode. Techniques to reconstruct the third dimension of tracks ( $\Delta z$ ) from the charge or PMT signal at the amplification region are also under development.

In addition, a cubic meter detector design is underway. This design consists of four TPC volumes and employs transparent mesh anodes.<sup>58</sup> The amplification region of each TPC pair is read out with a single set of CCD cameras. When filled with 75 Torr of  $\text{CF}_4$ , the cubic meter detector will contain 380 grams of target material. Given three months of live time (exposure  $\sim 0.1$  kg-year), this detector is capable of achieving the most stringent limit to date ( $10^{-38}$  cm<sup>2</sup>) on the spin-dependent WIMP-proton interaction (see Fig. 20).

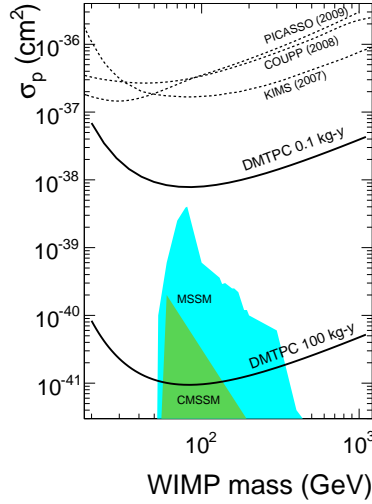


Fig. 20. Projected sensitivity for WIMP-proton spin-dependent interactions. A cubic meter detector filled with  $\text{CF}_4$  at 75 Torr with  $\sim 3$  months live time has an exposure of 0.1 kg-yr (upper solid line). The lower solid line indicates the sensitivity for a 100 kg-yr exposure, which cuts deep into the preferred MSSM parameter space. These projected sensitivities assume a threshold energy of 50 keV and less than one neutron-induced background event. For reference, one picobarn equals  $10^{-36} \text{ cm}^2$ .

## 5. NEWAGE – Long-term observation tests with a practical-sized $\mu$ -TPC in an underground laboratory

NEWAGE (NEw generation WIMP-search With an Advanced Gaseous tracking device Experiment) is a direction-sensitive dark matter search experiment with a gaseous micro-time-projection chamber ( $\mu$ -TPC) that began detector R&D in 2003,<sup>59</sup> and published the first direction-sensitive dark matter limits in 2007 (see Fig. 21).<sup>60</sup> We have been studying the detector background in the Kamioka Underground Observatory since 2007.<sup>61</sup>

### 5.1. Prototype detector and its performance

The NEWAGE-0.3a detector, the first version of the  $(0.3\text{m})^3$ -class prototypes, is a gaseous  $\mu$ -TPC filled with  $\text{CF}_4$  gas at 152 Torr. The effective volume and the target mass are  $20 \times 25 \times 31 \text{ cm}^3$  and 0.0115 kg, respectively. For details of the detector system and performance studies, see Ref. 61. A picture and schematic of the NEWAGE-0.3a detector are shown in Fig. 22 and Fig. 23, respectively. The NEWAGE-0.3a detector is read out by a  $30.7 \times 30.7 \text{ cm}^2$   $\mu$ -PIC. A  $\mu$ -PIC is one of the several types of micro-patterned gaseous detectors. By orthogonally-formed readout strips with a pitch of 400  $\mu\text{m}$ , the  $\mu$ -PIC can generate two-dimensional images.<sup>62</sup>

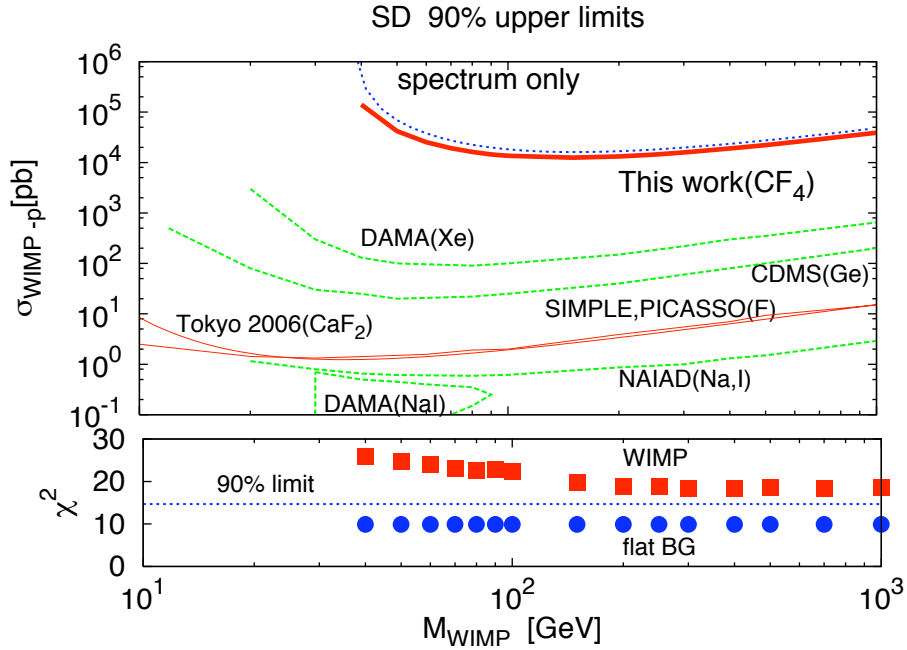


Fig. 21. First direction-sensitive WIMP-proton cross section limits (spin-dependent) set by NEWAGE-0.3a detector.<sup>60</sup>

The performance of the NEWAGE-0.3a detector measured in the underground laboratory is listed in Table 2 together with the projected goals. We show typical results demonstrating the capability of our method for direction-sensitive WIMP detection in Fig. 24 and Fig. 25. Three-dimensional nuclear tracks detected with the NEWAGE-0.3a detector are shown in Fig. 24. A dedicated data acquisition system with FPGA chips realizes the detection of clear three-dimensional tracks as successive digital hits. The right panel of Fig. 25 shows a “sky-map” image drawn by the detected nuclear tracks. We simply traced back the detected nuclear tracks on the map and the neutron source ( $^{252}\text{Cf}$ ) was clearly reconstructed in the image. The recoil angle distribution is shown in the left panel of Fig. 25 and the distribution was peaked at  $\cos\theta = 1$ . Detailed studies on fine tracks of fluorine nuclei are described in Ref. 61.

## 5.2. Background studies in an underground laboratory

We have been studying the detector performance and background in the Kamioka Observatory located at 2700m water equivalent underground since 2007.<sup>61</sup> The history of our underground activities is listed in Table 3.

Based on the background studies performed in the underground laboratory,<sup>63</sup> the most dominant source of background is  $\alpha$  particles that deposit a fraction of their

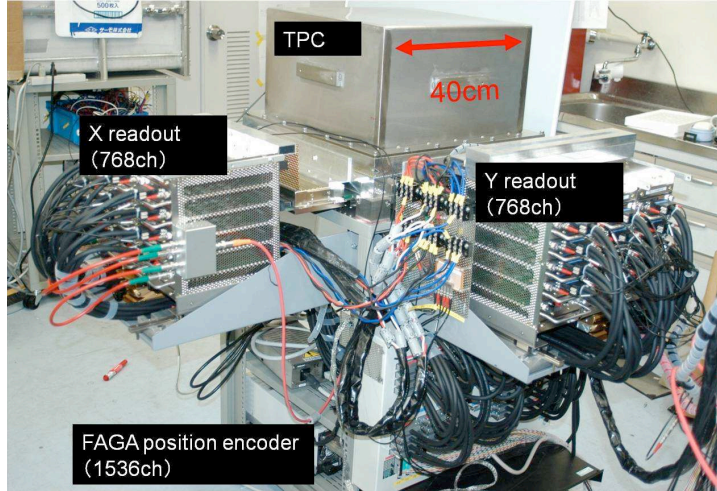


Fig. 22. Picture of the NEWAGE-0.3a detector.

Table 2. Current and goal performance of the NEWAGE-0.3a detector at the energy threshold.

Parameter	Value (present)	Value (goal)
Gas pressure [torr]	152	30
Energy threshold [keV]	100	35
Energy resolution [%] (FWHM)	70	30
$\gamma$ -ray detection efficiency	$8.1 \times 10^{-6}$	$1 \times 10^{-8}$
Nuclear track detection efficiency [%]	80	80
Nuclear track angular resolution (RMS)	$55^\circ$	$30^\circ$

Table 3. Accumulated exposure of the surface-run and underground-runs with NEWAGE-0.3a as of June 2009.

Run ID	Period	Exposure [kg-days]	Comment
Surface run	2006 Nov. 1st - 2006 Nov. 26th	0.151	first dark matter run <sup>60</sup>
Run1	2007 Mar. 6 - 2007 May. 15th	0.08	1/4 volume
Run2	2007 May. 15 - 2007 Aug. 6th	0.15	1/4 volume
Run3	2007 Dec. 7 - 2008 Jun. 9th	1.744	full operation
Run4	2008 Jun. 9 - 2008 Sep. 9th	0.602	BG study
Run5	2008 Sep. 11 - 2008 Dec. 4th	0.524	dark matter run <sup>63</sup>
Run6	2009 Mar. 2 - 2009 Jun. 24th	1.039	with gas circulation system (see Section 5.3)
Underground total		4.139	

energy in the gap volume between the  $\mu$ -PIC and the GEM. Although the alpha particles have energies of several MeV, these events can mimic low energy events because of the partial energy deposited in the small gap region (5 mm) without the electron-multiplication by the GEM. We will suppress these background events by

24 *Battat et al.*

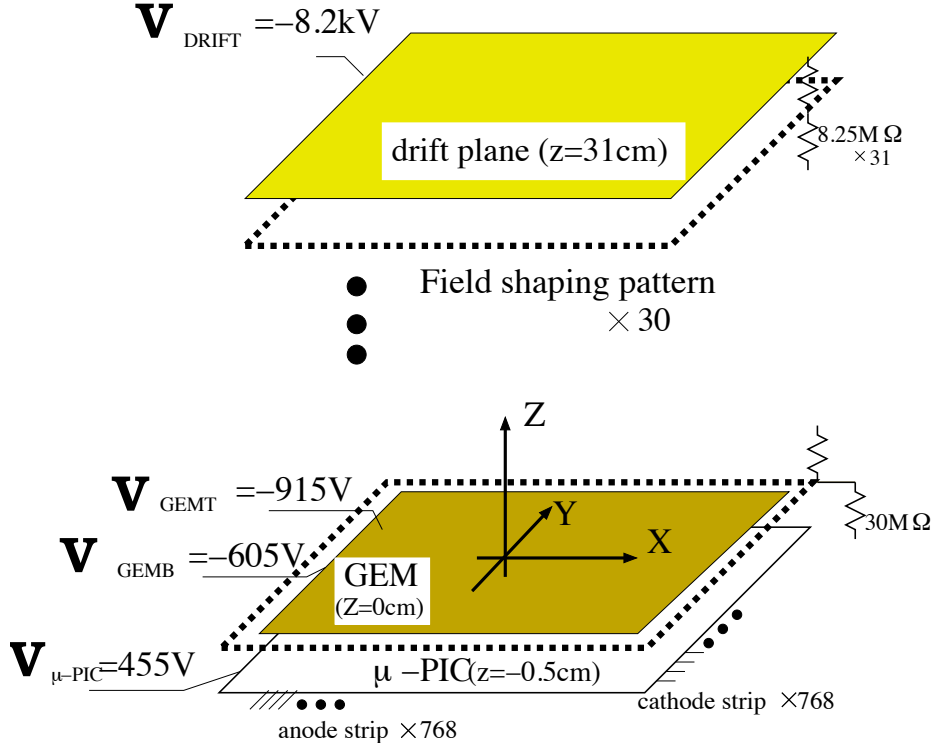


Fig. 23. Schematic view of the NEWAGE-0.3a detector. The volume between the drift plane and the GEM is the detection volume and is filled with  $\text{CF}_4$  gas at 152 Torr.

Table 4. Estimated background rates. The rates at the energy threshold are shown in units of [counts/kg/days/keV].

Source	Rate
Ambient gammas	$\sim 10$
Ambient fast neutrons	$\sim 10^{-1}$
Cosmic muon	$< 10^{-1}$
Internal $\alpha$ (fiducial volume)	$< 10^{-1}$
Internal $\alpha$ (gap volume)	$< 40$
Internal $\beta$	$< 5$
Measured (Run5)	50

replacing the detector components with radiopure materials.

### 5.3. Stability Improvement

In the beginning of 2009, we installed a gas circulation system which consists of a charcoal filter, getter pump, and Teflon bellows pump to maintain the gas purity for more than one month. We monitored the gas gain and the radioactive radon ( $^{220}\text{Rn}$ )



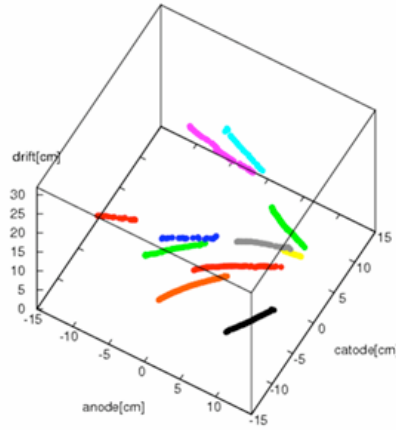


Fig. 24. Nuclear (proton) tracks detected with the NEWAGE-0.3a detector. This measurement was performed with a  $\text{CF}_4\text{-C}_4\text{H}_{10}(9:1)$  gas mixture at 152 Torr.

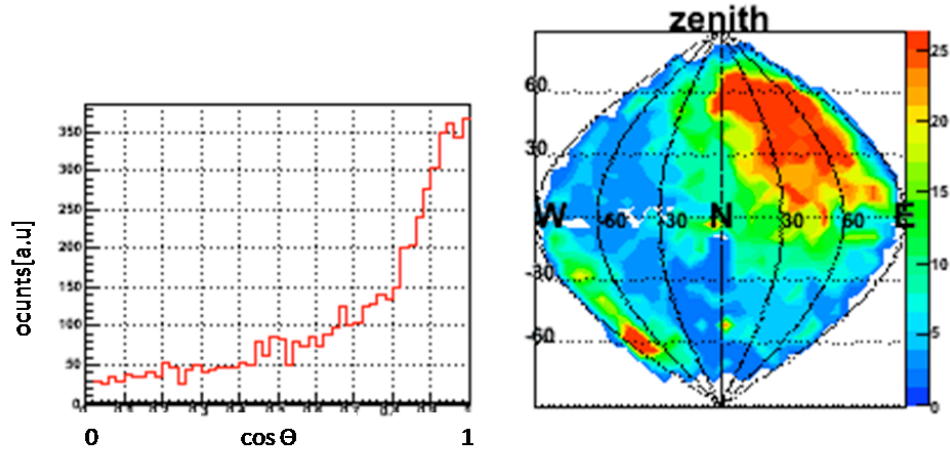


Fig. 25. Measured  $|\cos \theta|$  distribution (left) and the 2D map (right) of recoil tracks in the laboratory frame.  $\theta$  is the angle between the incoming neutron and the recoiling proton. This reaction roughly emulates WIMP-fluorine elastic scatterings. The  $^{252}\text{Cf}$  neutron source was positioned at 45 degrees East of North at an elevation of 35 degrees. This measurement was performed with a  $\text{CF}_4\text{-C}_4\text{H}_{10}(9:1)$  gas mixture at 152 Torr.

and  $^{222}\text{Rn}$ ) contamination in the gas using the high energy ( $\sim 6$  MeV) radon-progeny peaks. Monitored radioactive radon rates and gas gains are shown in the upper and lower panels of Fig. 26, respectively. Those monitored in the previous run (Run-5) are also shown for comparison. We found that the gas circulation system reduced the radon rate by a factor of five in 20 days and maintained the gas gain for twice

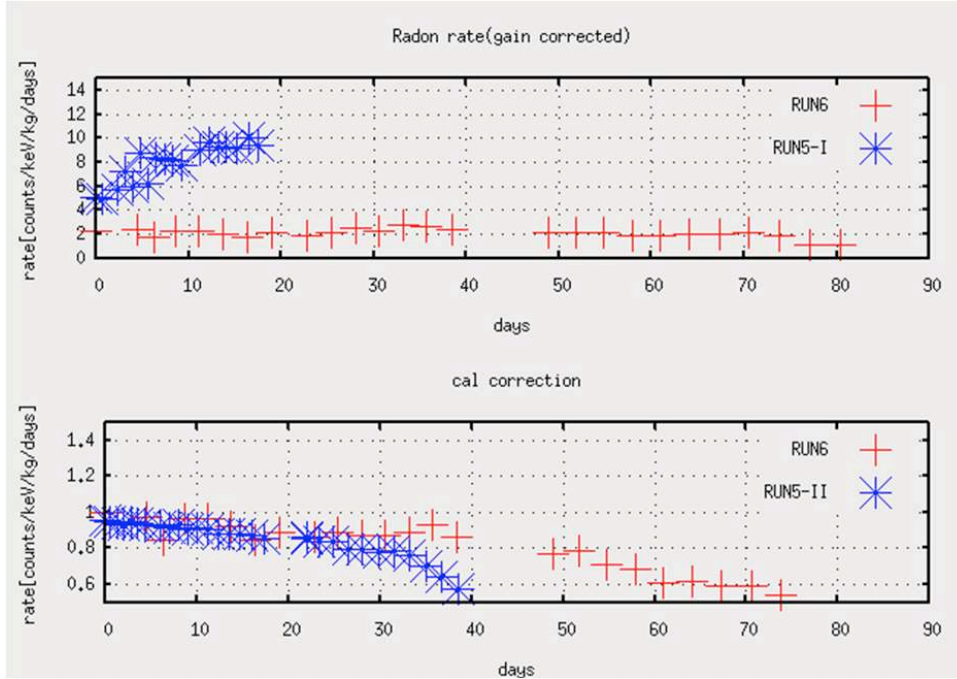


Fig. 26. Monitored radon progeny count rate and gas gains with (Run6) and without (Run5) the gas circulation system.

as long.

#### 5.4. Sensitivity Improvement and Scaling-up

We are improving the tracking algorithm in the online data acquisition system in order to improve the  $\gamma$ -ray rejection factor. Further algorithm improvements are planned to reconstruct the head-tail of the tracks. Our next prototype, NEWAGE-0.3b, with a detection volume of  $23 \times 28 \times 50 \text{ cm}^3$ , has started performance measurements in a surface laboratory. Our next step will be to assemble four  $\mu$ -PICs to form a  $60 \times 60 \text{ cm}^2$  tiled read-out area. We started to develop a pixel-read out ASIC named “QPIX,” for the ultimate readout system of the  $\mu$ -TPC.<sup>64</sup>

#### 5.5. NEWAGE Summary

Notable R&D results contributing to this international study so far are:

- We performed a direction-sensitive dark matter search measurement, analyzed the data, and set the first direction-sensitive limits. This means “the whole-chain” was performed not by a simulation but by a real experiment and supports our feasibility study in the final section.

- We employed a micro-patterned gas detector (MPGD), which is one of the strong candidates for the final huge detector, of a practical size ( $30.7 \times 30.7 \text{ cm}^2$ ) for the first time. We also have shown three-dimensional tracks can be detected with a dedicated electronics system. We are studying the scaling-up and background reduction issues of these MPGDs in a few years considering the cost-versus-sensitivity issues discussed in the final section.
- We have performed underground measurements for two years. R&D results, especially gas-circulation studies for long-term measurement, should be indispensable for a huge detector development.

We plan to develop a detector with a  $\sim 1 \text{ m}^3$  fiducial volume in a few years, and to determine the final design for a very large detector (multi-modules of the  $1 \text{ m}^3$  detector) taking account of the sensitivity and its cost.

## 6. A directional detector for non-baryonic dark matter search:

### MIMAC: (MIcro-tpc MAtrix of Chambers)

The MIMAC project is a multi-chamber detector for dark matter search, which aims to measure both tracks and ionization with a matrix of micromegas  $\mu$ TPC filled with  $^3\text{He}$ ,  $\text{CF}_4$ ,  $\text{CH}_4$  or/and  $\text{C}_4\text{H}_{10}$ . A 10 kg  $^3\text{He}$  dark matter detector, or the equivalent mass of  $\text{CF}_4$ , with a 1 keV threshold (MIMAC) would be sensitive to SUSY models allowed by present cosmological and accelerator constraints. This study highlights the complementarity of this experiment with most current spin-dependent experiments: proton based detectors and neutrino telescopes.

Using both  $^3\text{He}$  and  $\text{CF}_4$  in a patchy matrix of  $\mu$ TPCs opens the possibility to compare rates for two atomic masses, and to study separately the neutralino interaction with neutrons and protons, as the main contribution to the spin content of these nuclei is dominated by one nucleon. With low mass targets, the challenge is also to measure low energy recoils, below 6 keV for Helium, by means of ionization measurements. Low pressure operation of the MIMAC detector will enable the discrimination of the neutralino signal from backgrounds on the basis of track features and directionality.

The electron/nuclear recoil discrimination is based on track length, which is expected to be about ten times longer for an electron than for a nuclear recoil of the same energy. Identification of neutrons will be done by event time correlations between chambers, assuming that a WIMP will not interact twice in the whole MIMAC detector. Ultimately, the last background rejection tool is the reconstruction of the incoming direction of the particle. There are two steps when preparing a dark matter detector aiming at directional search:

- first, the energy of the recoil must be measured with accuracy, which implies a precise knowledge of the quenching factor,
- second, the possibility to reconstruct a 3D track must be shown. This is a

key point as the required exposure is decreased by an order of magnitude between 2D read-out and 3D read-out.<sup>65</sup>

Nonetheless, the energy threshold must be as low as possible, in the keV range or even sub-keV, owing to the exponential feature of the recoil spectrum.

We developed a  $\mu$ TPC prototype with a 16.5 cm drift length, read out by a bulk micromegas. At first, we used a standard 128  $\mu\text{m}$  bulk micromegas (non-pixelized anode plane) in order to measure the energy resolution of our detector. To correctly assess the real recoil energy on the nuclei, we performed a complete measurement of the ionization quenching factor in the energy range of dark matter search, i.e. below 10 keV.<sup>66,67</sup> In the following, we describe the Ionization Quenching Factor (IQF) measurements<sup>68</sup> and 3D track measurements realized by the MIMAC collaboration.

### 6.1. Ionization quenching measurements

The energy released by a nuclear recoil in a medium produces in an interrelated way three different processes: i) ionization, producing a number of electron-ion pairs, ii) scintillation, producing a number of photons coming from the de-excitation of quasi-molecular states and iii) heat produced essentially by the motion of nuclei and electrons. The way in which the total kinetic energy released is shared between the electrons and nuclei by interactions with the particle has been estimated theoretically four decades ago,<sup>69</sup> for very specific cases (those in which the particle and the target are the same). Since then, phenomenological studies have been proposed for many (particle, target) systems.<sup>70,71</sup> At low energies, in the range of a few keV, the ionization produced in a medium is strongly energy dependent, and systematic measurements are needed. In order to measure the ionization quenching factor for  $^4\text{He}$ ,  $^3\text{He}$ ,  $^1\text{H}$  and  $^{19}\text{F}$ , the LPSC has developed a dedicated facility producing light ions at energies of a few keV. This facility, called MIMAC's source (shown in Fig. 27), uses an Electron Cyclotron Resonance Ion Source (ECRIS)<sup>72,73</sup> and a Wien filter to select the desired charge-to-mass ratio with a high voltage extraction going up to 50 kV. This facility has enabled the first measurements shown in Fig. 28 confirming that there is sufficient ionization at low energies with  $^4\text{He}$  and  $^3\text{He}$ .<sup>68</sup>

In Fig. 28, the measurements at 350, 700, 1000 and 1300 mbar are shown.<sup>68</sup> We observe a clear, roughly linear, dependence of the IQF on the pressure of the gas that will be reported in a future study down to less than 100 mbar.

In summary, we have measured for the first time the ionization quenching factor of  $^4\text{He}$  down to very low energies showing the amount of ionization available from recoils of  $^4\text{He}$ . The IQF dependence on the pressure of the gas has been described for four different pressures. An estimation of the scintillation produced in the gas mixture as a function of the energy of the particles has been done. The IQF variation as a function of the quencher has been presented. These measurements are particularly important for searching WIMPs using  $^3\text{He}$  and in general to better understand the ionization response of helium gas detectors. For more details see Ref. 68.

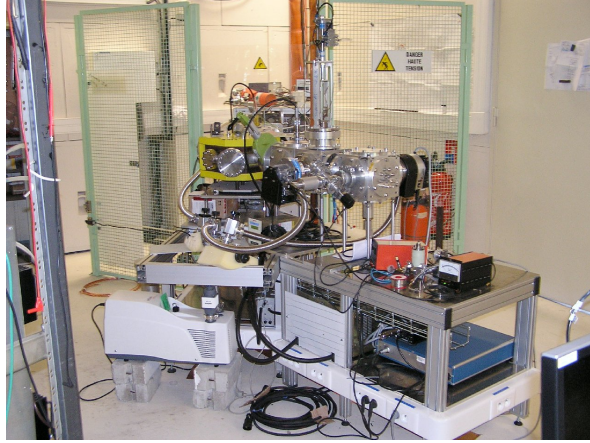


Fig. 27. Ionization Quenching Factor Facility at the LPSC Grenoble.

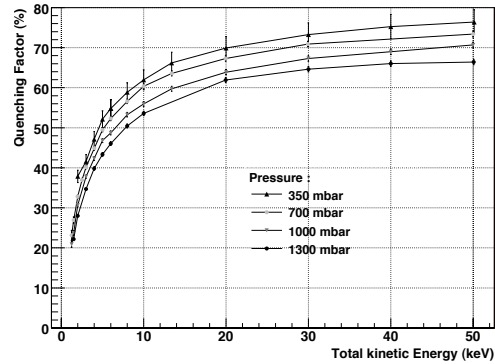


Fig. 28.  $^4\text{He}$  quenching factor as a function of  $^4\text{He}$  total kinetic energy (keV) for 350, 700, 1000 and 1300 mbar, in the case of  $^4\text{He}$  in  $^4\text{He} + 5\% \text{C}_4\text{H}_{10}$  mixture. Measured data are presented with error bars included mainly dominated by systematic errors. Straight line segments between experimental points help to separate the different series of measurements. From Ref 68.

## 6.2. Low recoil energy threshold

Because the number of expected WIMP events increases exponentially at low energies,<sup>11</sup> one of the most important detector parameters is the recoil energy threshold. We have measured, with a micromegas detector<sup>74,75</sup> taking into account the IQF previously measured,  $^4\text{He}$  recoils down to energies of 1 keV as shown in Fig. 29.

The electron energy resolution ranges from  $\sim 12\%$  ( $\sigma$ ) with an  $^{27}\text{Al}$  source, down to  $\sim 5\%$  for 5.9 keV electrons. Although a precise measurement of the energy of the recoil is the starting point of any background discrimination, the 3D reconstruction of the track is necessary to do dark matter directional detection.

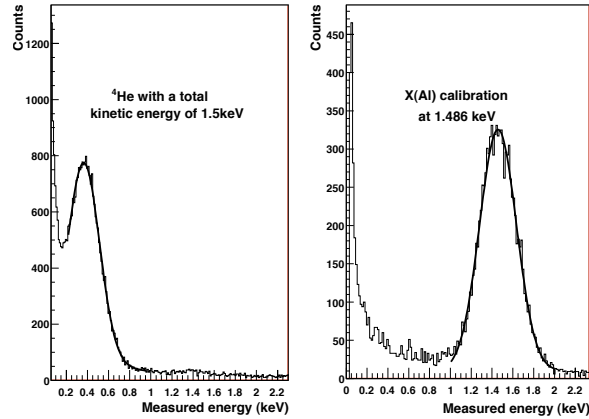
30 *Battat et al.*

Fig. 29. Spectra of 1.5 keV total kinetic energy  $^4\text{He}$  (left) and 1.486 keV X-ray of  $^{27}\text{Al}$  (right) in  $^4\text{He} + 5\% \text{C}_4\text{H}_{10}$  mixture at 700 mbar. The comparison of the energy measured between these two spectra gives the quenching factor of Helium in  $^4\text{He} + 5\% \text{C}_4\text{H}_{10}$  mixture at 700 mbar. From Ref. 68.

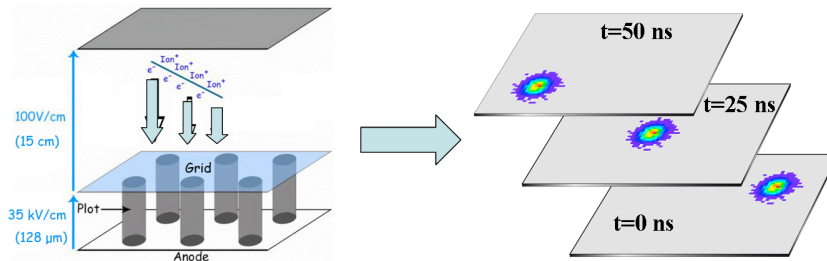


Fig. 30. Track reconstruction in MIMAC. The anode is scanned every 25 ns and the 3D track is reconstructed, knowing the drift velocity, from the series of images of the anode.

### 6.3. Three dimensional tracks with micromegas

The 3D reconstruction strategy chosen for the MIMAC project is the following: i) the electrons from the track are projected on the anode thus allowing to access information on x and y coordinates, ii) the anode is read every 25 ns, iii) knowing the drift velocity, the series of images of the anode allows to reconstruct the 3D track.

In order to reconstruct a few mm track in three dimensions, we use a bulk micromegas<sup>74,75</sup> with a  $3 \times 3 \text{ cm}^2$  active area, segmented in  $300 \mu\text{m}$  pixels. We use a 2D readout with  $424 \mu\text{m}$  pitch, in order to read both dimensions (x and y). This bulk is provided with a 325 LPI (Line Per Inch) woven micro-mesh made from  $25 \mu\text{m}$  stainless steel wire. The angular resolution of the recoil track reconstruction is  $\sim 15$  degrees (with energy dependence).

3D track reconstruction requires dedicated, self-triggering electronics, able to

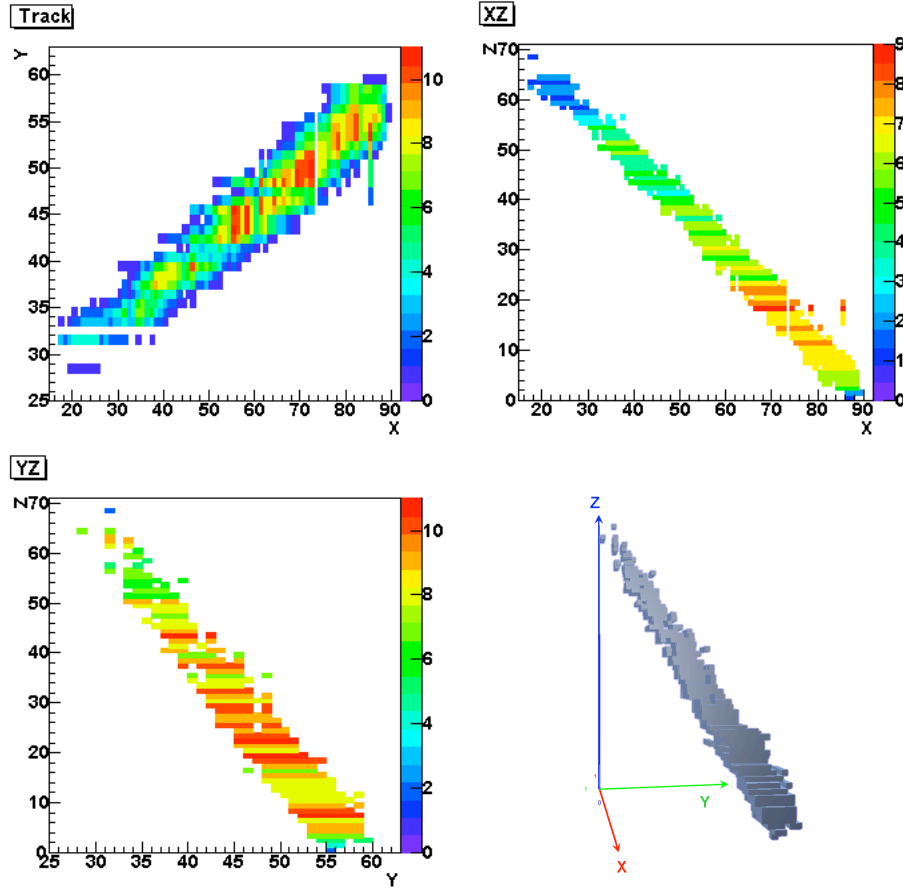


Fig. 31. The x-y, y-z and x-z projections of a 5.5 MeV alpha track (from  $^{222}\text{Rn}$ ) as seen by the MIMAC electronic and acquisition system. The z-coordinate is reconstructed from 25 ns scans of the x-y anode. The lower right panel presents a 3D view of the track. This high energy event will be used to evaluate the drift velocity in the gas mixture.<sup>77</sup>

sample at a frequency of 40 MHz.<sup>76</sup> To do so, the LPSC electronic team designed an ASIC in a  $0.35\ \mu\text{m}$  BiCMOS-SiGe technology. With an area approximately equal to  $1.5\ \text{mm}^2$ , this ASIC contains 16 channels, each having its own charge-sensitive preamplifier, current comparator and 5 bit coded tunable threshold. The 16 channels are sent to a mixer and a shaper to measure the energy in the ASIC. Each of the 12 ASICs is connected to FPGAs programmed to process, merge and time sort data. Finally, the electronics board is connected to an ethernet microcontroller which forwards the data via a TCP socket server to the acquisition station. This first version of the MIMAC ASIC has been running in the MIMAC prototype since May 2008. The next version, with 64 channels, is currently under development at the LPSC and will be ready before the end of 2009.

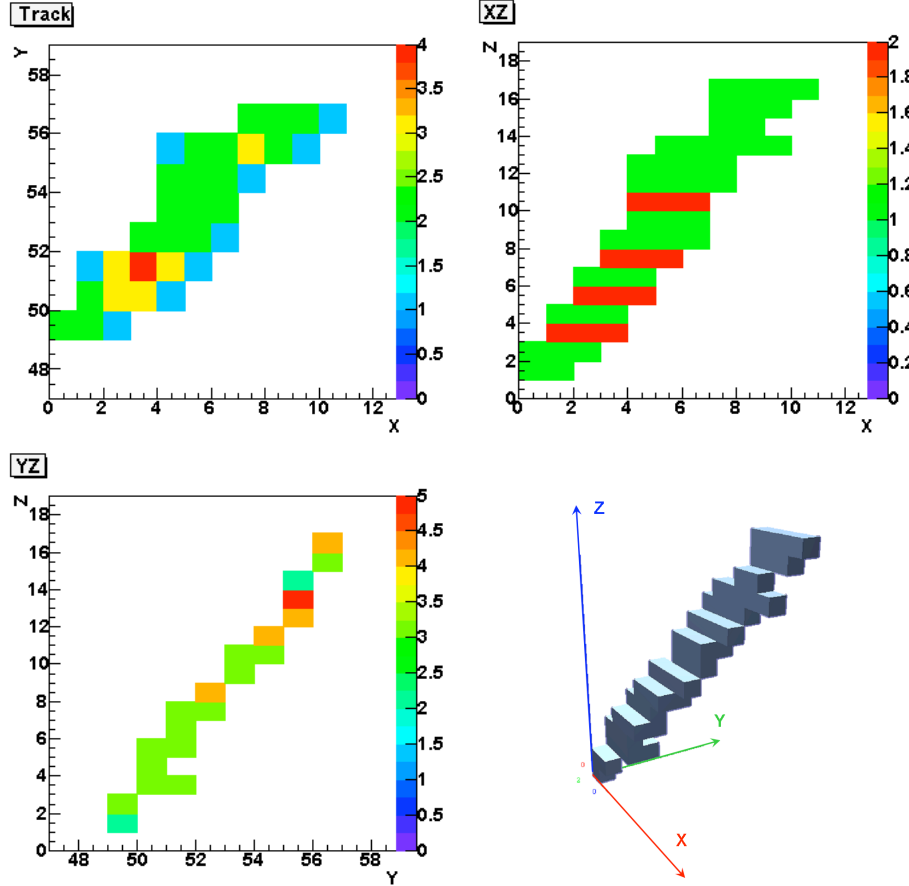
32 *Battat et al.*

Fig. 32. The x-y, y-z and x-z projections of a 5.9 keV electron track as seen by the MIMAC electronic and acquisition system. The z-coordinate is reconstructed from 25 ns scans of the x-y anode. The lower left panel presents a 3D view of the track. The volume of a pixel is  $424 \times 424 \times 400 \mu\text{m}^3$ , the size in z being driven by the scanning time (25 ns) and the electron drift velocity ( $16 \mu\text{m}/\text{ns}$  in this case).

Fig. 31 presents a 5.5 MeV alpha track (from  $^{222}\text{Rn}$ ), obtained in  $^4\text{He} + 5\% \text{C}_4\text{H}_{10}$  mixture at 350 mbar. Although at higher energy than needed for dark matter detection, this event shows the quality of the 3D reconstruction. The upper left panel presents the projection on the anode (x-y plane) and the lower right panel presents the 3D track, the z-coordinate being reconstructed with the strategy described above. 5.5 MeV alpha tracks from  $^{222}\text{Rn}$  will be used to evaluate the drift velocity in various mixtures of interest for directional dark matter detection.

Fig. 32 presents a reconstructed 5.9 keV electron track, obtained in  $^4\text{He} + 5\% \text{C}_4\text{H}_{10}$  mixture at 350 mbar. This is the first low-energy track in MIMAC. Both the length (8 mm), and the angle ( $\phi, \theta$ ) are reconstructed. The lower right panel presents a 3D view of the track. The volume of a pixel is  $424 \times 424 \times 400 \mu\text{m}^3$ , the size in z



being driven by the scanning time (25 ns) and the electron drift velocity (16  $\mu\text{m}/\text{ns}$  in this case). This event is of particular interest as it is a typical background event for dark matter. The correlation of the measured energy and the 3D reconstructed track length allows us to discriminate nuclear recoils from background.

#### 6.4. MIMAC summary

MIMAC has successfully measured recoils through ionization at the low energies of interest for WIMP detection. We have developed a specific chip giving access to a 3-D track reconstruction with a 300 microns spatial resolution. We are ready to scale-up the prototype to a 1 m<sup>3</sup> in the framework of an international collaboration.

### 7. Nuclear Emulsions

Nuclear emulsions allow for both tracking resolution and large target mass, which has great potential for directional dark matter detection. Emulsions are photographic films composed of AgBr and gelatin that can be used as 3D tracking detectors with  $\sim 1 \mu\text{m}$  resolution. This resolution is essential for the detection of short life-time particles, for example the tau neutrino,<sup>78</sup> double hyper nucleus<sup>79</sup> and so on. Recent analyses of nuclear emulsions are all automated,<sup>80</sup> which enables large-scale experiments. For example, OPERA,<sup>81</sup> a neutrino oscillation experiment at Gran Sasso, Italy, uses 30,000 kg of emulsions.

Nuclear emulsions may be useful in a directional dark matter search if they can detect the nuclear recoil tracks from WIMP interactions with sufficient accuracy. The high density ( $\sim 3 \text{ g}/\text{cm}^3$ ) of emulsions, and extremely high resolution are the strongest points. From SRIM, the expected range of a WIMP-induced nuclear recoil track is on the order of 100 nm. However, it is difficult to detect nuclear recoil tracks in standard emulsions because the maximum resolution is about 1  $\mu\text{m}$ . Therefore, we developed a new high-resolution nuclear emulsion, called the “Nano Imaging Tracker” (NIT).<sup>82</sup> In the NIT, the AgBr crystal size is  $40 \pm 9 \text{ nm}$  and the density is  $2.8 \text{ g}/\text{cm}^3$ . The density of AgBr that an incoming particle can penetrate is 11 AgBr/ $\mu\text{m}$  (Fig. 33).

#### 7.1. Test of nuclear recoil track direction

By using low-velocity Kr ions instead of nuclear recoils, the ability to reconstruct the nuclear recoil detection was determined. With an electron microscope, the track, which extended over several emulsion grains, could be observed (Fig. 34), and the detection efficiency was measured to be more than 90%. The measured range was consistent with SRIM simulation.<sup>82</sup>

#### 7.2. Optical detection of nuclear recoil track

When we consider a dark matter search, it is not realistic to use an electron microscope to scan a large volume of emulsions. Furthermore, nuclear recoil tracks which

34 *Battat et al.*

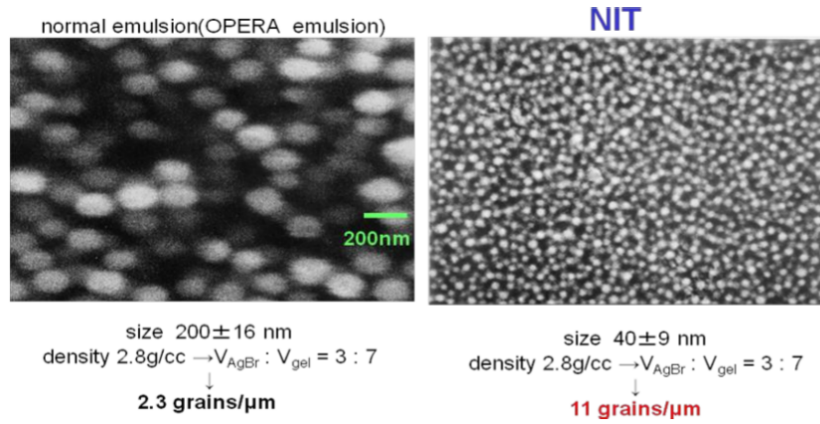


Fig. 33. Electron microscope image of standard emulsion (left) and NIT emulsion (right)

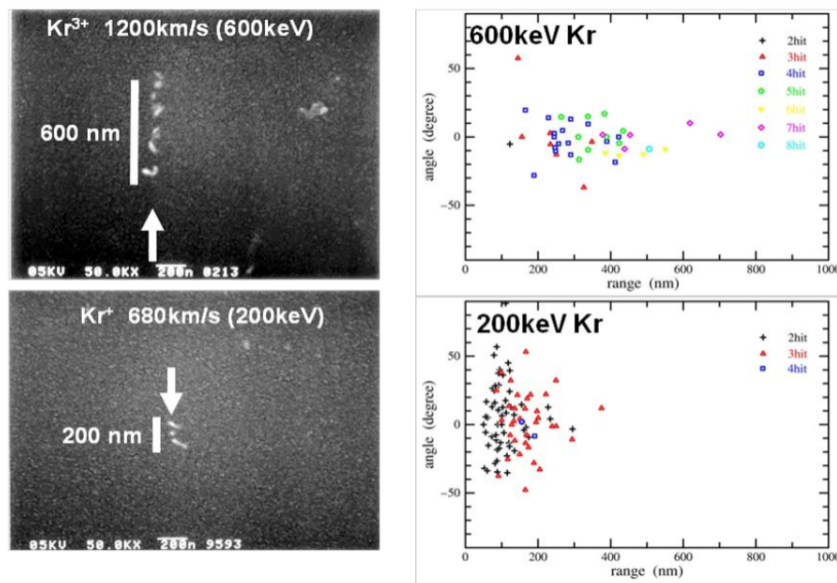


Fig. 34. (left) Electron microscope image of Kr ion track (600 keV and 200 keV) and (right) track data.

are less than  $1 \mu\text{m}$  long (smaller than the optical resolution) cannot be identified as tracks by an optical microscope. To resolve this problem, a method was developed to expand the tracks. Nuclear recoil tracks consist of grains spanning roughly 100 nm. If the emulsion is then expanded, the inter-grain spacing grows and the track length is expanded to several  $\mu\text{m}$ . With this technique, nuclear recoil tracks may be identified by an optical microscope. Here, we used a pH-controlled chemical treatment to

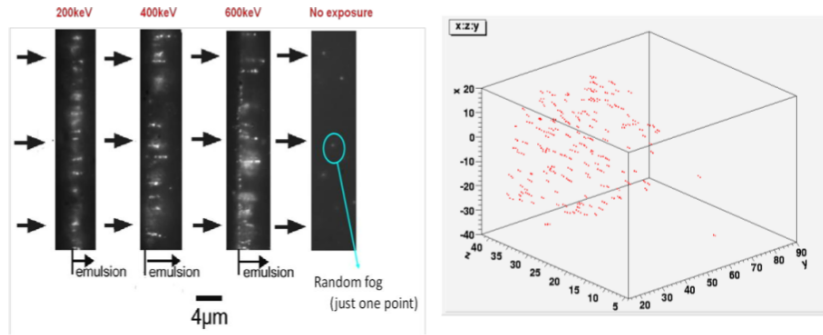


Fig. 35. (left) Optical microscope image of expanded Kr ion track (200, 400, 600 keV and reference). (right) 3D tracking data for expanded Kr ion track (600 keV).

expand the emulsion. As a result, tracks from Kr ions with  $E > 200$  keV attained lengths of several  $\mu\text{m}$ , and could be recognized as tracks by an optical microscope.<sup>83</sup> Such tracks could be distinguished from random noise (fog) because the fog consists of single grain events (see Fig. 35). The angular resolution of the original state for NIT is about 12 degrees or better. However, the angular resolution is expected to be about 45 degrees with the expansion technique. In practice, if the expansion technique is used, two or more NIT emulsion detectors should be mounted in the directions horizontal and vertical to Cygnus on an equatorial telescope.

### 7.3. Background rejection

We can discriminate electrons and  $\gamma$  from nuclear recoils by their different  $dE/dx$  values. Because the sensitivity of nuclear emulsions usually depends on the  $dE/dx$  of the incoming particle, by controlling the sensitivity of the emulsion itself and the power of the development treatment, electrons with low  $dE/dx$  will not appear in the emulsion. In the present state, the estimated electron rejection power is  $10^5$  or better using new sensitized chemical treatment (Halogen Acceptor sensitization).<sup>84</sup> Moreover, we expect to improve this sensitivity control of the development treatment. For alphas, serious background sources are U, Th chain and Rn. Since these energies are on the order of MeV, nuclear emulsions can identify the alpha track with 3D range discrimination. This means that alphas are not backgrounds for emulsions by at least fiducial cut. Neutrons are expected to be the main background. With sensitivity control of the development treatment, neutron recoil tracks which have low  $dE/dx$  may be rejected, but, finally they are rejected by directionality.

### 7.4. Sensitivity for WIMP searches

The sensitivity of nuclear emulsions to WIMPs is estimated with a Monte Carlo simulation. For zero background events, a 1000 kg-year exposure, and 100 nm range threshold ( $\sim 100$  keV energy threshold for Ag, Br recoils), the sensitivity is expected

to be better, by about one order of magnitude, than the current XENON10 limit.<sup>10</sup> In addition, by using higher resolution NIT (for example, 20 nm AgBr size), the range threshold would be 50 nm and the sensitivity would improve further by one order of magnitude.

### 7.5. *Future Planning*

Currently, we are developing the new readout system and emulsion production facility. In addition, in recent R&D efforts, we are studying large nuclear stopping power using a dedicated development treatment. This will enable more background rejection and head-tail discrimination. We aim to put these developments into practice and start running a 1 kg prototype within two years.

## 8. TPC Readout with Gas Electron Multipliers and Silicon Pixels

Directional dark matter detection may benefit from recent advances in detector technologies at particle colliders. One option is to read out Time Projection Chambers with silicon strip or silicon pixel detectors. This approach is used by NEWAGE (Section 5), MIMAC (Section 6), and Lawrence Berkeley National Laboratory (LBNL) (this section). While a silicon based readout is costly per unit readout area, it can offer full 3-D reconstruction of nuclear recoils, ionization measurement in each detector element, and low threshold operation. As a result this approach to TPC readout should improve both background rejection and WIMP signal sensitivity, and may prove competitive in terms of total detector cost for comparable sensitivity.

### 8.1. *LBNL TPC Prototype Device*

The LBNL group has developed a small TPC prototype device where the ionization charge is amplified with Gas Electron Multipliers (GEMs) and read out with pixel Integrated Circuit (IC) chips.<sup>85</sup> This allows 3-D reconstruction of tracks in the TPC drift volume. The GEMs used were purchased from CERN, while the pixel chip used was the FE-I3 pixel chip from the ATLAS experiment at the LHC. This pixel chip was designed for the high event rates and high radiation dose at the LHC, but its pixel size ( $50 \times 400 \mu\text{m}$ ) and operating frequency (40 MHz) happen to match the spatial and timing resolution requirements set by directional dark matter detection with low pressure gas TPCs. By measuring ionization in each pixel, the pixel chip also provides a measurement of  $dE/dX$ , which is needed for background suppression when detecting WIMPs,

### 8.2. *Measured Performance with Cosmic Rays*

The performance of the prototype device was measured with cosmic rays, and seems very promising. By using two GEM layers, it was possible to achieve both large gains (up to 40,000 with Ar/CO<sub>2</sub>) and stable operation. Fig. 36 shows a simulated avalanche in one of the GEM layers. The pixel chip has very low noise ( $\sim 120$

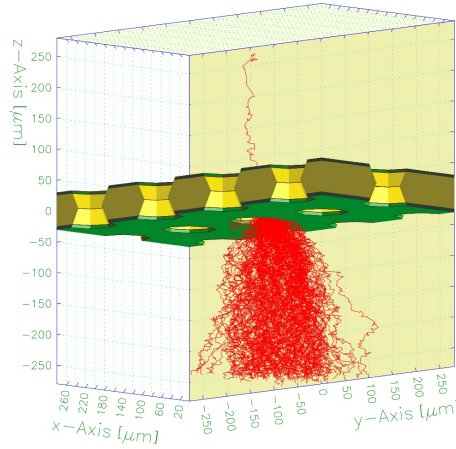


Fig. 36. A simulated avalanche produced by a single electron passing through a single GEM. With 500 V across the GEM, this event has a multiplication factor of 258. Only the electrons contributing to the effective avalanche gain are shown.

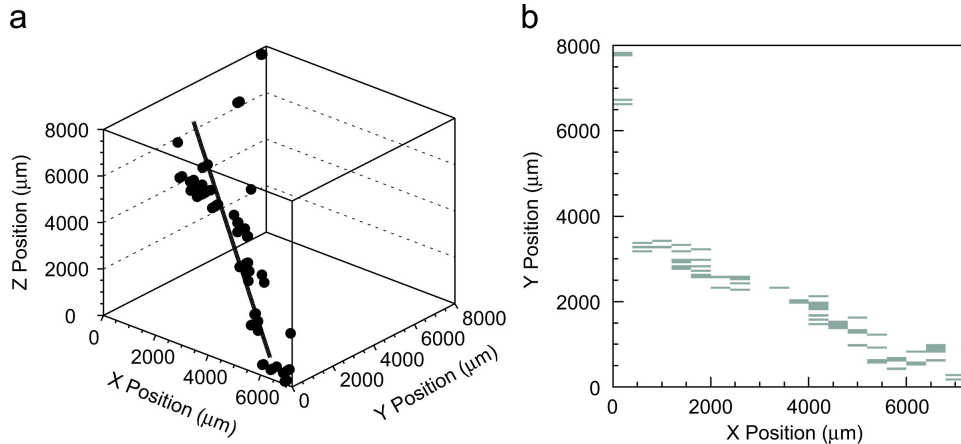


Fig. 37. A typical cosmic ray event. (left) The event reconstructed in 3-D space. Each point represents a hit in the pixel chip, and the line is a result of a fit to these points. The x-y position of each point is given by the center of mass of the corresponding hit pixel, and the z position given by the arrival time of the hit. (right) Raw readout of the pixel chip for the same event. Each filled rectangle represents a  $50 \times 400 \mu\text{m}$  silicon pixel where a hit was recorded.

electrons), compared with a typical operating threshold of 2-5000 electrons. Reconstructed charged tracks yield an x/y/z point resolution of  $130/70/150 \mu\text{m}$  when operating with Ar/CO<sub>2</sub> gas at atmospheric pressure (these are the readout resolutions, after subtracting the estimated diffusion in quadrature). Fig. 37 shows a typical example track found in a cosmic ray event.

### 8.3. *Applicability to WIMP Searches*

Of particular relevance to dark matter detection is that the prototype device appears capable of reading out all the primary ionization charge, even single electrons, with efficiency close to unity. That means one should be able to reach a very low energy threshold when reconstructing nuclear recoils from WIMP/nucleon collisions. The FE-I3 pixel chip buffers hits until a trigger occurs, and pixels without hits do not generate data. Thus demands on a downstream data acquisition system should be relatively light in the case of WIMP detection.

Several critical issues need more study and work before this technology can be applied to directional WIMP dark matter detection. For instance, the ATLAS pixel chip is currently limited to reading out 16 consecutive time intervals of 25 ns, which limits the size of drift volume (along the drift direction) that can be read out. This part of the chip design may need to be modified for directional dark matter detection. One also needs to demonstrate that the GEMs can operate without sparking or serious aging problems when using gases and pressures more suitable for directional dark matter detection.

## 9. Development of low-background micromegas readout planes for directionality experiments

In micropattern readouts, metallic strips or pads, precisely printed on plastic supports using photolithography techniques (much like printed circuit boards), are used in place of wires to receive drifting charge produced in the gas. Micropattern readouts are more simple, robust and mechanically precise than conventional wire planes.

Detectors based on this concept, first introduced by Oed in 1988,<sup>86</sup> are called Micro-Pattern Gas Detectors (MPGD). Thus far, several designs employing different multiplication structures have been proposed, with varying levels of success (Microstrip, Microwire, Microgap, Microdots (micropin), Microwell, Gas Electron Multiplier (GEM), etc.). Here, we focus on one of the most promising MPGDs: the Micromesh Gas Structure or micromegas.<sup>75</sup>

The micromegas concept, created about 14 years ago and actively developed since then by the CEA/Saclay group led by I. Giomataris, consists of a micromesh held  $\sim 50$ -100 microns away from the strip plane by insulating spacers. This geometry defines a high electric field gap in which an electron avalanche is produced, as in parallel plate chambers, inducing signals in both the mesh and the strips. The resulting avalanche topology can be imaged with unprecedented spatial resolution: a 2D readout pitch of  $300 \mu\text{m}$  is used in the CERN Axion Solar Telescope (CAST), and small prototypes with  $50 \mu\text{m}$  pixels exist. The micromegas concept is already employed in many particle physics experiments, and unique temporal, spatial and energy resolutions have been demonstrated (temporal resolutions below 1 ns, and spatial resolutions of at least  $17 \mu\text{m}$  have been achieved,<sup>87</sup> and an energy resolution of less than 11% FWHM for the 5.9 keV  $^{55}\text{Fe}$  peak is routinely achieved with

state-of-the-art micromegas planes).

In the field of rare events, the use of micromegas readouts have been pioneered by the Saclay and Zaragoza groups for CAST. Since 2002, CAST has employed a low-background micromegas detector. In 2007, two additional ones replaced the multiwire TPC. CAST has been a testing ground for micromegas technology. Ongoing efforts have produced three generations of detectors (regarding the fabrication method, detector materials, shielding and electronics and data reduction treatment), each with improved background levels.

Current micromegas readouts profit from the *bulk* method of fabrication,<sup>74</sup> in which the micromesh is imprinted into the readout itself using photolithography techniques. This improves the device's durability. In the latest generation of CAST detectors, the so-called *microbulk* micromegas developed by CERN/Saclay, the readout plane is fabricated from double-clad kapton foils, thereby increasing the gap precision and the gain stability and energy resolution of the detector. These improvements come at the cost of losing a bit of robustness and potential maximum area of fabrication with respect to the bulk fabrication technique.

An R&D program dedicated to developing high radiopurity micromegas is currently being pursued by the Zaragoza group. In the first phase, measurements of micromegas planes are being performed in the ultra-low background facilities of the Canfranc Underground Laboratory (LSC). Promising preliminary results indicate that *microbulk* readouts fabricated from radiopure raw materials exhibit lower levels of radiopurity per unit surface area (at the level of 0.1 mBq/cm<sup>2</sup> for U/Th) than competing readouts used in very low background experiments (e.g. low-background photomultiplier tubes or avalanche photodiodes), even in the absence of specific radiopurity development. In subsequent phases of this project, the aim is to identify traces of radioactivity and try to further reduce them by better choosing raw materials or by reducing contamination introduced by the manufacturing processes.

These tasks are part of a larger R&D effort, led by the Zaragoza and Saclay groups, which studies several aspects of the new generation of detectors for their application in other rare event experiments. Among other things, exhaustive studies of the energy resolution capabilities of *microbulk* micromegas are being done.<sup>88</sup> In addition, the development of multiplexed patterns is under exploration. This would reduce the number of channels required to read out large detector areas with high spatial resolution.

This work is part of the demonstration of scaling-up strategies which are essential for large directional WIMP detectors, and which includes the possibility of building single readouts of medium-large size, without losing the performance shown in the small prototypes. Along this line, *bulk* micromegas have been already built at the m<sup>2</sup> scale in the context of other projects,<sup>89</sup> though operational *microbulk* micromegas have been built only at the few tens of cm<sup>2</sup> scale.<sup>90,91</sup> Currently, a 30 × 30 cm<sup>2</sup> *microbulk* is being built to test and push the capability of current manufacturing techniques towards larger areas. Alternatively, *mosaic* micromegas schemes are be-

ing devised to instrument large readout areas with minimal dead zones. Finally, the previously mentioned multiplexing schemes are to be implemented in these large area readouts.

To conclude, micromegas detectors are under active development. An increasingly important portion of this R&D effort focuses on low background systems that would be a promising readout option for large-scale gas TPCs for directional WIMP detection.

## 10. Directional detector scale-up feasibility study

We now provide a qualitative discussion of the feasibility of a large scale directional TPC in relation to the state of the art. We summarize the main factors concerning a design, and highlight some critical-path issues needing further R&D or design work.

### 10.1. Cost Arguments

First, it is important to note that the total cost per unit sensitivity must be a primary factor in a design strategy. This point is particularly important for directional dark matter detectors because, when comparing with non-directional large-scale experiments, the cost drivers are not necessarily obvious. For instance, the need to use low pressure gas (leaving aside for now any prospect of solid state devices, such as emulsions) implies a detector of relatively large volume (possibly up to  $10^3$ - $10^4$  m<sup>3</sup> for spin-independent sensitivity) and hence an underground cavern larger than is within the experience of the conventional non-directional dark matter community. However, it is likely incorrect to assume that size itself is a major issue of concern, let alone a showstopper. Neither cavern excavation nor mechanical construction are likely to be major cost drivers for a large-scale directional detector.

Quantifying the sensitivity goal for a directional concept requires a different philosophy since, unlike non-directional detectors, the objective is not just to achieve a hint of a signal (or a limit) but to show clearly that events are of galactic origin. This would be unambiguous evidence for the existence of WIMP dark matter. A useful sensitivity parameter for comparison purposes is to determine, for a given WIMP type, interaction cross section, and distribution in the galactic halo, the minimum number of WIMP events  $N_W$  required to demonstrate to 95% C.L. that the distribution of recoil directions is not isotropic in the galactic frame, and hence cannot be of terrestrial origin. For instance, for the standard halo model, assuming 3D reconstruction with sense determination in an idealised detector with 20 keV recoil threshold, and accounting for basic gas physics such as straggling, it has been shown that  $N_W \sim 10$ .<sup>12</sup> For a practical detector it is likely that  $N_W \gg 10$  (if, for instance, there is only 2D reconstruction or no sense determination, depending on the detector design).

There is a cost tension between  $N_W$  and target mass, two parameters that likely scale very differently. For instance, investing in a new technology that reduces  $N_W$  by a factor of 2, such as by improving the position resolution with better



readout technology, is clearly only reasonable if the cost is less than that of doubling the target mass with the same readout technology. The latter might be a better option, depending on the absolute sensitivity required. Either way, the scale required implies that more work is needed to produce lower cost readout, electronics and mechanical infrastructure, though less so if the DAMA signal proves correct, in which case a much smaller detector would be sufficient. In fact, in this situation (e.g. if the DAMA signal can be explained by inelastic scattering), then the low-pressure gas TPC technology has significant advantages thanks to its particle tracking and identification ability for both electrons and nuclear recoils.

### 10.2. *Directional capability cost benefit*

Recent advances, many described in this work, have shown that there is some head-tail discrimination in low pressure gases. Thus, any of the current readout technologies, be it MWPCs, micropixel or CCD optics etc, could in principle cover a full spectrum of directionality capability as follows: (i) simple 1D readout with sense (head-tail discrimination), (ii) 2D readout with or without sense, (iii) 3D readout, with or without sense, (iv) all of the previous with or without absolute 3D event location (fiducialisation), i.e.  $\Delta x$ ,  $\Delta y$ ,  $\Delta z$  and absolute  $x$ ,  $y$ ,  $z$ . The first option may appear a poor bet. Indeed, 1D sensitivity (say  $z$ -projection in a gas TPC via timing information only) without sense, is probably ruled out completely. However, the forward-backward asymmetry signal for dark matter is so powerful that, depending on the extent to which head-tail discrimination can be realised, it is possible to envisage a scenario in which the funds that would have been used to build expensive 2D ( $x$ - $y$ ) readout planes are better used simply to build more target mass with 1D sensitivity, overcoming the implied loss in  $N_W$ . The main issue with this option is then how to maintain the necessary high background rejection (see Section 10.3). Pure 2D readout alone, as provided by current generation CCD technology, may also not be sufficient without the introduction of head-tail discrimination. Full 3D reconstruction of tracks provides a potential option even without head-tail. However, while the MWPC technology has approached 3D reconstruction, at least one of the dimensions is restricted in resolution by the wire spacing, currently 2 mm but potentially 1 mm. The micropixel readout has demonstrated full 3D reconstruction with position resolution  $< 1$  mm in all directions, but only at small scale ( $\sim 10$  cm) and relatively larger cost, without head-tail discrimination.

### 10.3. *Background rejection*

While it may be possible to reduce the scale-up cost for a given sensitivity by saving on the readout tracking capability, compensating this by increased target mass, in practice will depend also on the background rejection capability, particularly of gammas, low energy alphas and, most notably, radon progeny recoils (RPRs). The extreme case is 1D readout (case (i) above). For instance, the use of simple non-pixelated anode planes severely reduces the  $dE/dx$  discrimination capability and

introduces a degeneracy for certain orientations of particle tracks. The situation is less severe with simple 2D projection readout, as in the basic CCD option. However, one remaining issue is the degeneracy between short high  $dE/dX$  tracks and long low  $dE/dX$  tracks that happen to be oriented nearly perpendicular to the readout plane. Full 3D reconstruction, as provided by (e.g.) measuring the temporal profile of the induced charge on the 2D readout plane can break this degeneracy and improve background rejection. However, there still remains the issue of identifying low energy events from the detector walls. Radon progeny recoils, the low energy recoils from decay of radon daughters like  $^{218}\text{Po}$  deposited on surfaces by radon, have been identified as a severe issue here, since they can mimic WIMP events.<sup>39</sup> Low energy alphas, from U, Th contamination, arising when most of the alpha energy has been lost in the walls prior to emerging into the gas, are also a challenge.

Elimination of such events requires measurement of the absolute 3D position of events within the target volume, i.e.  $x$ ,  $y$  and  $z$  information - i.e. 3D fiducialisation. Implementation of such fiducialisation is well established in 2 dimensions ( $x$ - $y$ ), because the track position is measured relative to the  $x$ - $y$  edges for any pixilated 2D  $x$ - $y$  readout. However, without a measurement of the absolute  $z$  of an event, RPRs from the central high voltage cathode are the most insidious background events in directional TPCs.

Significant  $z$ -fiducialisation can be obtained from the pulse shape information encoded in the induced charge signals on the TPC electrodes. Ionization products from RPR events at the cathode must travel the entire drift length and will suffer greater diffusion, and therefore produce longer pulse shapes. This method of RPR rejection, however, is not perfect since there is a degeneracy with track orientation. New techniques are under investigation by several groups to achieve the necessary full  $z$ -fiducialisation. In summary, taking account of the concepts in Sections 10.1-10.3, it is likely that a large-scale directional detector will need 3D fiducialization, at least 2D directional reconstruction, and head-tail discrimination.

#### 10.4. *Intrinsic background, shielding, and site choice*

The efficiency required to achieve the background discrimination and  $z$ -fiducialisation described in Section 10.3 depends on the intrinsic level of background achievable. This has two aspects: (i) passive and active shielding to reduce external backgrounds, including the rock overburden in an underground laboratory, and (ii) material purification to reduce internal backgrounds, particularly from radon and neutrons. The requirements for the former have been well investigated.<sup>36</sup> The intrinsic insensitivity of the low pressure TPC technique to gammas means requirements for external high-Z passive shielding (Pb, Cu) are much reduced compared to conventional detectors. It is for this reason that first and second generation DRIFT detectors were constructed with no gamma shielding. However, the more sensitive detectors of the future will likely require some gamma shielding, depending on the capability to measure  $dE/dx$ . Hence, given the low mass-to-volume ratio of a low

pressure TPC and the absolute size needed, and unlike the case for conventional detectors, it is worth specifically seeking an underground site that has intrinsically the lowest possible gamma background, to save on gamma shielding costs. This means a site in salt is rather well suited to a large TPC. Salt sites have the lowest U, Th content but also, unlike the requirements for other proposed very large detectors such as for proton decay, a large directional TPC can be designed with an elongated shape, the type preferred in salt for geotechnical reasons. So a deep salt site could be rather well suited to a TPC. On the other hand, conventional sites, such as the proposed DUSEL, likely have other benefits that can impact positively on cost, for instance lower maintenance requirements. These issues need careful study.

As with all dark matter detectors, neutron backgrounds are likely the greatest challenge. However, the low mass-to-volume ratio for a TPC relative to conventional detectors makes neutrons a particular issue because the possibility of rejection by detection of multiple scatters is reduced, and backscattering within the volume is increased.<sup>49</sup> Concerning muon-induced neutrons, this implies that the underground site should likely be deeper than required for conventional detectors, or alternatively that an external neutron veto be used. This requirement may be partially mitigated if sensitivity to EM radiation (low  $dE/dx$ ) is maintained as a means of internally vetoing muon induced showers. Reduction of the neutron flux from radioactivity in the surrounding rock is better understood and can be achieved at modest cost using either polyethylene pellets, high-H walling material, or perhaps water shielding. However, neutrons from contamination of detector construction materials and components are more problematic, as in conventional direct detection experiments. The vessel structure is likely an important factor, however other components will also need careful selection, for instance the insulator material used in micromegas, and the optics in the case of CCD readout. Concerning radon and RPRs, the active fiducialisation being developed to mitigate this will not have 100% efficiency. Hence selection of detector materials with very low radon emanation rates as well as radon getters in the gas system will be necessary.

### **10.5. *Engineering and infrastructure limits***

Excavation of large caverns underground is well understood even at the scale required for a megaton proton decay experiment. A directional TPC would likely not require such a large cavern. Taking the example of SuperK, such a cavern could accommodate a directional target mass of order 10 tons, even at 40 Torr. At the known typical excavation cost of \$20-50 per m<sup>3</sup>, this implies a cost of  $\sim$  \$250k per ton of directional target. Excavation is thus unlikely to be a cost driver. Taking as the limit to feasibility an excavation comparable with a future proton decay experiment, we can obtain an upper limit target mass of order 400 tons, allowing for some increase in pressure. This could be capable of directional detection at  $10^{-11}$  pb dark matter interaction cross section without sense determination. More realistic in the near-term are the proposed excavation modules at DUSEL, which can provide

sufficient space for a competitive first stage target mass.

Regarding engineering structures, though large by dark matter standards, there are no cryogenics necessary and few physics constraints on geometry. Most important is the need for radiopurity and capability to limit outgassing of impurities, including radon daughters.

### **10.6. *Data Acquisition and readout***

This area is likely to be a (or the) major cost driver. For example, a 1 ton target at 40 Torr and 2 mm resolution would require  $\sim 10^7$  readout channels for a charge readout concept, each requiring fast ADC output. Allowing for increased pressure and better position resolution could see this rise to  $10^9$  channels per ton. However, use can be made of the expected short recoil track lengths to allow grouping of channels, yielding a reduction to say  $\sim 10^6$  channels. In this scenario, track reconstruction is maintained and an internal fiducial volume defined to exclude edge events, but there is degeneracy in the absolute position of accepted events. Grouping of this form is performed in DRIFT and is under development for micropixel readout. Development of new chips could be important here to suppress costs per channel, but careful design with current technology may provide significant cost savings. The CCD option would require of order 10,000 CCD cameras per ton plus associated optics, unless some similar form of multiplexing or grouping can be found. Otherwise, the concept would maintain absolute position information in 2D. A significant issue for charge readout is also the design of the cabling and associated feeds to pre-amplifiers outside the vessels.

### **10.7. *Target gas systems, remote operation and search strategy***

The use of  $\text{CF}_4$ ,  $\text{CS}_2$  negative ion gases, plus mixtures and additives of other target gases including He, is quite well understood at small scale now. It has been demonstrated that  $\text{CF}_4$  works with  $\text{CS}_2$ , such that the low diffusion capability of the negative ion gas technology works with F as a target. Remote and safe operation has been shown with  $\text{CS}_2$  and  $\text{CF}_4$  in  $1 \text{ m}^3$ , demonstrating that requirements for operations staff can be minimal. So far gases have generally been flowed through vessels and vented to atmosphere through filters. However, for large-scale detectors, in order to reduce costs and to reduce the need for disposal systems, recirculation, with radon and impurity removal, and/or long-term operation with vessels sealed is probably essential. Work is underway on this by multiple groups.

One advantage of using a gas TPC is the possibility of easily changing the target nuclei and target density (pressure) while using the same detector apparatus. This opens the possibility of various search strategies, including both spin-dependent and spin-independent in the same detector. One possibility also is to start at high pressure first, say 400 Torr, to increase the target mass and hence sensitivity to events, maintaining recoil discrimination but without directional information. Work

is needed here to understand the discrimination capability vs. pressure and gas mixture. Use of multiple targets and multiple sites simultaneously may have advantages.

### 10.8. *Health and safety*

Health and safety is a major consideration for any experiment, however no show-stoppers have so far been identified for a large directional TPC. We can make use of extensive experience from previous and planned large underground experiments. The main novel issue is gas handling and high voltages, with their (relatively low) potential for asphyxiation or accidental creation of poisonous or explosive mixtures. All these issues have been addressed by existing experiments. Larger volumes will require larger ventilation systems, but these are well within current mine technology. A road tunnel site might require more stringent investigation because of the proximity of the general public. The use of large quantities of  $\text{CF}_4$  needs special care given its nature as a greenhouse gas.

### 10.9. *Costs, timescales and main areas of future work*

It is possible to estimate the cost and timescale for construction of a large-scale experiment by extrapolating from current technology. For instance, construction of a single  $1 \text{ m}^3$  DRIFT module of the current design, including commercial DAQ and shielding is now  $\sim \$50\text{k}$ . This is dominated by the electronics and vessel construction. Extrapolating from this, making reasonable assumptions on cost savings through use of mass produced electronics, larger unit vessels, gas recirculation and other scaling factors, yields  $\sim \$150\text{M}$  per ton of target. Additional shielding, such as a neutron veto or passive gamma shield, could significantly increase this if a suitable deep and low background site is not available. Development of the field indicates that such a detector will be required within 6 – 8 years, either to prove that a signal seen in a non-directional detector is not simply an unidentified terrestrial background, or because directionality will be needed to reject possible neutrino-induced backgrounds.

To meet this challenge we can identify several key issues from above that require further research before a large scale design can be finalized:

- demonstration of a technique to completely fiducialize the detector volume
- demonstration that intrinsic radon related background can be sufficiently reduced
- demonstration that low background outer vessels are possible
- demonstration of bulk gas recirculation and cleaning
- optimization of readout vs. target mass for best cost/sensitivity benefit

## 11. Acknowledgements

The production of this document was inspired by the Cygnus 2009 workshop on directional dark matter detection at the Massachusetts Institute of Technology (MIT)

in Cambridge, Massachusetts, USA. We would like to thank the National Science Foundation, the MIT Kavli Institute for Astrophysics and Space Research and the MIT Laboratory for Nuclear Science for their generous financial support of the workshop.

The DMTPC collaboration acknowledges the support of the Advanced Detector Research Program of the U.S. Department of Energy, the National Science Foundation, the Reed Award Program, the Ferry Fund, the Pappalardo Fellowship program, the MIT Kavli Institute for Astrophysics and Space Research, and the MIT Physics Department.

The NEWAGE collaboration wishes to acknowledge the support of Grant-in-Aids for KAKENHI (19684005) of Young Scientist(A); JSPS Fellows; and Global COE Program “The Next Generation of Physics, Spun from Universality and Emergence” from Ministry of Education, Culture, Sports, Science and Technology (MEXT) of Japan.

The MIMAC collaboration acknowledges ANR-07-BLAN-255 funding.

The Emulsions work was supported by the Global COE Program of Nagoya University, “Quest for Fundamental Principles in the Universe (QFPU)” from JSPS, and MEXT of Japan.

This manuscript has been authored by an author at Lawrence Berkeley National Laboratory under Contract No. DE-AC02-05CH11231 with the U.S. Department of Energy. The U.S. Government retains, and the publisher, by accepting the article for publication, acknowledges, that the U.S. Government retains a non-exclusive, paid-up, irrevocable, world-wide license to publish or reproduce the published form of this manuscript, or allow others to do so, for U.S. Government purposes.

## References

1. G. Bertone, D. Hooper and J. Silk, *Phys. Rept.* **405**, 279 (2005).
2. G. Jungman, M. Kamionkowski and K. Griest, *Phys. Rept.* **267**, 195 (1996).
3. G. Kane and S. Watson, *Mod. Phys. Lett.* **A23**, 2103 (2008).
4. M. W. Goodman and E. Witten, *Phys. Rev.* **D31**, p. 3059 (1985).
5. PAMELA, O. Adriani *et al.*, *Nature* **458**, 607 (2009).
6. J. Chang *et al.*, *Nature* **456**, 362 (2008).
7. The Fermi LAT, A. A. Abdo *et al.*, *Phys. Rev. Lett.* **102**, p. 181101 (2009).
8. R. J. Gaitskill, *Ann. Rev. Nucl. Part. Sci.* **54**, 315 (2004).
9. CDMS, Z. Ahmed *et al.*, *Phys. Rev. Lett.* **102**, 011301 (2009).
10. XENON, J. Angle *et al.*, *Phys. Rev. Lett.* **100**, p. 021303 (2008).
11. J. D. Lewin and P. F. Smith, *Astropart. Phys.* **6**, 87 (1996).
12. B. Morgan, A. M. Green and N. J. C. Spooner, *Phys. Rev.* **D71**, p. 103507 (2005).
13. J. D. Vergados and A. Faessler, *Phys. Rev.* **75**, 055007 (2007).
14. A. K. Drukier, K. Freese and D. N. Spergel, *Phys. Rev.* **D33**, 3495 (1986).
15. K. Freese, J. A. Frieman and A. Gould, *Phys. Rev.* **D37**, p. 3388 (1988).
16. DAMA, R. Bernabei *et al.*, *Eur. Phys. J.* **C56**, 333 (2008).
17. D. N. Spergel, *Phys. Rev.* **D37**, p. 1353 (1988).
18. C. J. Copi, J. Heo and L. M. Krauss, *Phys. Lett.* **B461**, 43 (1999).
19. D. Stiff and L. M. Widrow, *Phys. Rev. Lett.* **90**, p. 211301 (2003).

20. D. P. Finkbeiner, T. Lin and N. Weiner, *arXiv/0906.0002* (2009).
21. D. Tucker-Smith and N. Weiner, *Phys. Rev.* **D64**, p. 043502 (2001).
22. F. Mayet *et al.*, *Phys. Lett.* **B538**, p. 257 (2002).
23. E. Moulin, F. Mayet and D. Santos, *Phys. Lett.* **B614**, 143 (2005).
24. P. Gondolo *et al.*, *JCAP* **0407**, p. 008 (2004).
25. C. J. Martoff *et al.*, *Nucl. Instrum. Meth.* **A440**, 355 (2000).
26. T. Ohnuki, D. P. Snowden-Ifft and C. J. Martoff, *Nucl. Instrum. Meth.* **A463**, 142 (2001).
27. DRIFT, G. J. Alner *et al.*, *Nucl. Instrum. Meth.* **A535**, 644 (2004).
28. DRIFT, B. Morgan *et al.*, *Nucl. Instrum. Meth.* **A513**, 226 (2003).
29. DRIFT, G. J. Alner *et al.*, *Nucl. Instrum. Meth.* **A555**, 173 (2005).
30. DRIFT, S. Burgos *et al.*, *Astropart. Phys.* **31**, 261(May 2009).
31. C. J. Martoff *et al.*, *Nucl. Instrum. Meth.* **A555**, 55 (2005).
32. J. Miyamoto *et al.*, *Nucl. Instrum. Meth.* **A526**, 409 (2004).
33. P. K. Lightfoot *et al.*, *Astropart. Phys.* **27**, 490 (2007).
34. B. Morgan *et al.*, *Astropart. Phys.* **23**, 287 (2005).
35. DRIFT, S. Burgos *et al.*, *Astropart. Phys.* **28**, 409 (2007).
36. M. J. Carson *et al.*, *Nucl. Instrum. Meth.* **A546**, 509 (2005).
37. DRIFT, S. Burgos *et al.*, *Nucl. Instrum. Meth.* **A600**, 417 (2009).
38. <http://www.youtube.com/watch?v=G4270rjtDnY>.
39. DRIFT, S. Burgos *et al.*, *Nucl. Instrum. Meth.* **A584**, 114 (2008).
40. D. Muna, Three dimensional analysis and track reconstruction in the DRIFT-II dark matter detector, PhD thesis, University of Sheffield, (Sheffield, UK, 2008).
41. N. J. Spooner, *J. Phys. Soc. Jap.* **76**, p. 111016 (2007).
42. P. Majewski *et al.*, *arXiv/0902.4430* (2009).
43. D. P. Snowden-Ifft *et al.*, *Nucl. Instrum. Meth.* **A516**, 406 (2004).
44. R. Battesti *et al.*, *Lect. Notes Phys.* **741**, 199 (2008).
45. DRIFT, S. Burgos *et al.*, *JINST* **4**, p. P04014 (2009).
46. H. R. Crane, *Rev. Sci. Inst.* **32**, 953 (1961).
47. K. Pushkin and D. Snowden-Ifft, *Nucl. Instrum. Meth.* **A606**, 569 (2009).
48. H. M. Araujo, V. A. Kudryavtsev, N. J. C. Spooner and T. J. Sumner, *Nucl. Instrum. Meth.* **A545**, 398 (2005).
49. V. A. Kudryavtsev, N. J. C. Spooner and J. E. McMillan, *Nucl. Instrum. Meth.* **A505**, 688 (2003).
50. R. Lemrani *et al.*, *Nucl. Instrum. Meth.* **A560**, 454 (2006).
51. H. M. Araujo *et al.*, *Astropart. Phys.* **29**, 471 (2008).
52. M. Robinson *et al.*, *Nucl. Instrum. Meth.* **A511**, 347 (2003).
53. E. Tziaferi *et al.*, *Astropart. Phys.* **27**, 326 (2007).
54. DMTPC, D. Dujmic *et al.*, *J. Phys. Conf. Ser.* **120**, p. 042030 (2008).
55. DMTPC, T. Caldwell *et al.*, *arXiv/0905.2549* (2009).
56. DMTPC, A. Kaboth *et al.*, *Nucl. Instrum. Meth.* **A592**, 63 (2008).
57. DMTPC, D. Dujmic *et al.*, *Nucl. Instrum. Meth.* **A592**, p. 123 (2008).
58. DMTPC, D. Dujmic *et al.*, *Astropart. Phys.* **30**, 58 (2008).
59. T. Tanimori *et al.*, *Phys. Lett.* **B578**, 241 (2004).
60. NEWAGE, K. Miuchi *et al.*, *Phys. Lett.* **B654**, 58 (2007).
61. NEWAGE, H. Nishimura *et al.*, *Astropart. Phys.* **31**, 185 (2009).
62. A. Takada *et al.*, *Nucl. Instrum. Meth.* **A573**, 195(April 2007).
63. H. Nishimura, Direction-sensitive direct dark matter search experiment with a gaseous TPC, PhD thesis, Kyoto University, (Kyoto, Japan, 2009).
64. A. Matsuzawa *et al.* Proceedings of TIPP09, (2009), Tsukuba, Japan.

48 *Battat et al.*

65. A. M. Green and B. Morgan, *Astropart. Phys.* **27**, 142(March 2007).
66. O. Guillaudin *et al.*, *J. Phys. Conf. Ser.* **179**, 012012(July 2009).
67. F. Mayet *et al.*, *J. Phys. Conf. Ser.* **179**, 012011(July 2009).
68. D. Santos *et al.*, *arXiv/0810.1137* (2008).
69. J. Lindhard *et al.*, *Mat. Fys. Medd. Dan. Vid. Selsk.* **33(14)**, 1 (1963).
70. A. Hitachi, *Rad. Phys. Chem.* **77**, 1311 (2008), note: The W-value for CF<sub>4</sub> used in this reference was too large. The proper value of 34.3 eV (G.F. Reinking *et al.*, *J. Appl. Phys.* 60, 499, 1986) makes the ionization 1.57 times the values (the right axis) shown in Fig. 7 of this reference.
71. J. Ziegler *et al.*, <http://www.srim.org>.
72. T. Lamy *et al.*, in preparation.
73. R. Geller, *Electron cyclotron resonance ion sources and ECR plasmas* (Institute of Physics Publishing, Philadelphia, 1996).
74. I. Giomataris *et al.*, *Nucl. Instrum. Meth.* **A560**, 405 (2006).
75. Y. Giomataris, P. Rebourgeard, J. P. Robert and G. Charpak, *Nucl. Instrum. Meth.* **A376**, 29 (1996).
76. J. P. Richer *et al.*, in preparation.
77. F. Mayet *et al.*, in preparation.
78. DONuT, K. Kodama *et al.*, *Phys. Rev.* **D78**, p. 052002 (2008).
79. S. Aoki *et al.*, *Prog. Theor. Phys.* **85**, 951 (1991).
80. S. Aoki *et al.*, *Nucl. Instrum. Meth.* **B51**, 466 (1990).
81. R. Acquafredda *et al.*, *JINST* **4** (2009).
82. M. Natsume *et al.*, *Nucl. Instrum. Meth.* **A575**, 439 (2007).
83. Emulsions, T. Naka *et al.*, *Nucl. Instrum. Meth.* **A581**, 761 (2007).
84. K. Kuge *et al.*, *J. Imaging Science and Tech.* **53(1)**, 010507 (2009).
85. T. Kim *et al.*, *Nucl. Instrum. Meth.* **A589**, 173 (2008).
86. A. Oed, *Nucl. Instrum. Meth.* **A263**, 351 (1988).
87. J. Derré and I. Giomataris, *Nucl. Instrum. Meth.* **A477**, 23 (2002).
88. T. Dafni *et al.*, *Nucl. Instrum. Meth.* **A608**, 259 (2009).
89. S. Anvar *et al.*, *Nucl. Instrum. Meth.* **A602**, 415 (2009).
90. P. Abbon *et al.*, *New Journal of Physics* **9**, 170 (2007).
91. S. Aune *et al.*, *J. Phys. Conf. Ser.* **179**, 012015 (2009).